Economic Geology
Vol. 96, 2001, pp. 1775–1797

Mineralogic and Stable Isotope Zonation at the Surface over the El Salvador Porphyry Copper Deposit, Chile

YASUSHI WATANABE†

Institute for Geo-Resources and Environment, AIST, Central 7, Higashi 1-1-3, Tsukuba, 305-8567 Japan

AND JEFFREY W. HEDENQUIST

99 Fifth Avenue, Suite 420, Ottawa, Ontario, K1S 5P5, Canada

Abstract

We examined in detail the mineralogic and stable isotope characteristics of alteration minerals exposed at the surface of the El Salvador porphyry copper deposit. A total of 276 samples was collected from 203 localities over an area of >5 km^2 at elevations between 2,900 and 3,300 m. The alteration assemblages can be separated into two groups, broadly corresponding to the stages previously identified from underground studies, although the early stage K silicate alteration identified underground is not evident at the surface. A transitional to late stage is characterized at the surface by assemblages of (1) muscovite-andalusite with trace diaspore (including some areas rich in andalusite) and (2) muscovite with trace diaspore. There is a sharp contact outward with a marginal propylitic assemblage (chlorite-calcite-epidote). Pyrophyllite occurs as a retrograde overprint of muscovite in both of the transitional to late-stage assemblages. These assemblages are concentrically zoned and centered on a core of least-altered granodiorite porphyry, a late intramineral intrusion. The muscovite-andalusite assemblage occurs up to 500 m away from the granodiorite porphyry, and andalusite-rich zones are located near the brecciated margin of the porphyry. Further outward is the muscovite zone, from 500 to 1,500 m wide. The pyrophyllite overprint overlaps the contact of the muscovite-andalusite and muscovite zones, and occurs mainly above 3,000 m elevation, such that its present distribution is controlled largely by topography. Very late alteration minerals occur in radial pebble dikes of hydrothermal breccia and their extensions, and they are dominated by an advanced argillic assemblage of alunite-(± aluminum phosphate-sulfate minerals)-diaspore-zunyite-pyrophyllite-dickite, with residual muscovite. In one case a breccia extends upward and appears to be the root of a 300 × 500 m outcrop, 80 m thick, of massive quartz-alunite replacement of rhyolite.

Pure mineral separates were prepared from these samples for O, H, and S isotope analysis, including 48 samples of silicate minerals (muscovite, pyrophyllite, dickite, and supergene kaolinite), and 20 samples of alunite, some supergene in origin. Information on mineral assemblage was used to estimate temperatures of formation, which then allowed calculation of the isotopic composition of associated hydrothermal fluids. The fluid responsible for forming the muscovite had a relatively narrow range of isotopic composition, 6.5 ± 1.5 per mil $\delta^{18}O$ and –40 ± 10 per mil δD. The heaviest $\delta^{18}O$ and δD values, about 8 and –35 per mil, respectively, were obtained from the samples with andalusite-muscovite-diaspore assemblage. This composition is close to that expected for a magmatic fluid, with <10 to 20 percent meteoric-water component responsible for forming the other muscovite samples. The fluid compositions calculated for the very late stage alunite range from 5 and –30 per mil to –1 and –40 per mil $\delta^{18}O$ and δD, respectively. This range in composition agrees with the trend predicted for magmatic vapor absorbed by local groundwater, the latter similar in composition to that responsible for forming the supergene kaolinite. There is no systematic spatial zonation of the alunite samples in terms of isotopic composition or paleotemperature. The temperature estimates from S isotope geothermometry are higher than those based on mineral assemblage, possibly caused by partial supergene replacement of some hypogene alunites.

There is no strong isotopic zonation of hydrothermal minerals from surface alteration assemblages at El Salvador that can be applied to generate clear exploration guidelines. By contrast, mapping of alteration mineralogy in the field, backed up by laboratory checking of mineralogy and examination of relict minerals and replacement textures in thin section, clearly indicates the center of the late intramineral intrusion.

Introduction

WE PRESENT the results of a detailed examination of the mineralogic and stable isotope characteristics of hydrothermal alteration assemblages at the surface over the El Salvador porphyry copper orebody, Chile (Fig. 1). Our goal is to better understand the zonation of surface alteration assemblages and their isotopic compositions and to identify guidelines of possible use for exploration. Experience in mapping porphyry copper deposits has shown several features that can assist in their assessment. (1) The abundance of early quartz veinlets typically matches the contour of hypogene copper (Clode et al., 1999), if the level of erosion is sufficiently deep to expose veins. (2) The distribution of supergene glassy limonite, goethite, hematite and jarosite assemblages reflects the underlying sulfide assemblages and abundance (Anderson, 1982). (3) The patterns of sulfide zoning can be reconstructed from reflected-light study of relict sulfides trapped in quartz (Gustafson and Hunt, 1975). In addition, these deposits have large halos of zoned alteration assemblages that are useful in defining the position within the overall porphyry system (Lowell and Guilbert, 1970). However, such halos are commonly complicated by an alteration overprint that may mask

†Corresponding author: e-mail, y-watanabe@aist.go.jp

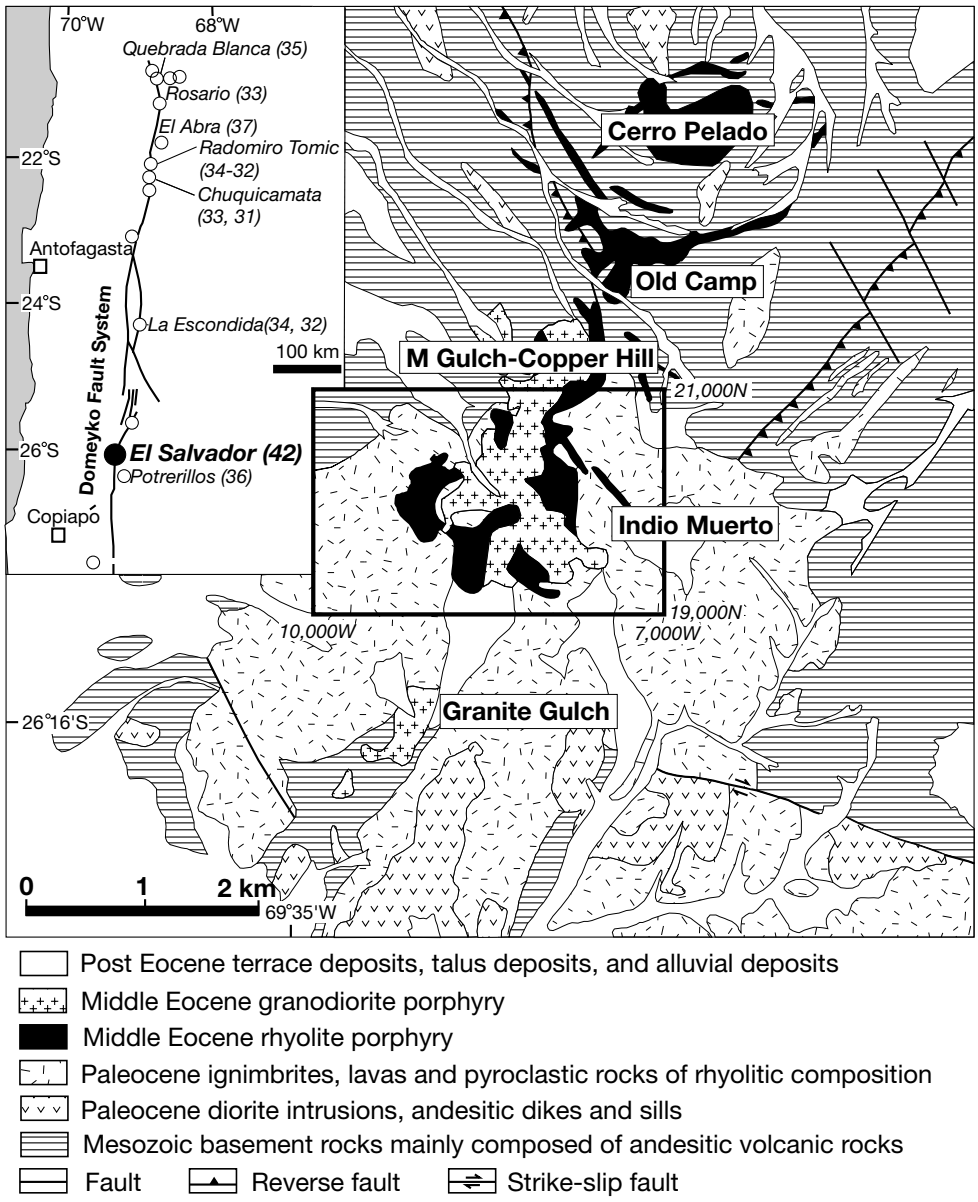

FIG. 1. Location map showing the El Salvador deposit and other porphyry deposits (ages in Ma) in northern Chile (modified from Clark et al., 1998), with a simplified geologic map of the El Salvador district, centered on the Indio Muerto area (from Cornejo et al., 1997).

the indicators of buried ore, as the result of intramineral intrusions (Kirkham, 1971) and/or supergene processes.

We selected the El Salvador deposit for several reasons, including the fact that there is a broad halo of well-exposed alteration assemblages, >5 km^2 in area, with leached capping outcrops up to 3,300 m elevation. The geology of the deposit and products of alteration and mineralization have been studied extensively (Gustafson and Hunt, 1975; Gustafson and Quiroga, 1995), and the geology and geochronology of the district are relatively well understood (Cornejo et al., 1997; Gustafson et al., 2001). The distribution of ore zones is well known from underground workings and drilling, and there is a good library of samples from areas that are now inaccessible at surface. Our results confirm that detailed geologic mapping and related study of alteration assemblages coupled with stable isotope analysis over porphyry prospects contributes to understanding the subsurface geometry of the systems and their hydrothermal evolution, an aid to efficient prospect assessment.

Background and previous studies

The assemblages, zoning, and paragenesis of the hydrothermal minerals of porphyry orebodies (Lowell and Guilbert, 1970; Sillitoe, 1973), as well as the hydrothermal evolution of porphyry systems (e.g., Sheppard et al., 1969, 1971; Gustafson and Hunt, 1975; Hedenquist et al., 1998) have long been studied. Combining these studies with laboratory results (e.g., Hemley et al., 1980; Hemley and Hunt, 1992) has

provided an understanding of the genesis of the porphyry alteration assemblages, leading to an improved ability to explore for and detect concealed porphyry deposits. The history of study and present understanding of the origin of porphyry deposits were reviewed by Hunt (1991) and Hedenquist and Richards (1998), and references therein.

One of the arguments regarding the genesis of porphyry ore involves the nature of the hydrothermal fluid related to the sericitic and advanced argillic assemblage. Sheppard et al. (1969, 1971) and Taylor (1974, 1997) concluded that the solutions responsible for the phyllic minerals are dominated by meteoric water, on the basis of oxygen and hydrogen isotope data from porphyry deposits in North America. In contrast, Kusakabe et al. (1990) suggested that the fluids that formed phyllic assemblages at El Teniente and Rió Blanco in Chile were magmatic in origin. Hedenquist et al. (1998) studied the Far Southeast porphyry and Lepanto epithermal Cu-Au deposits in the Philippines. They concluded that K silicate and advanced argillic assemblages were coupled in origin and formed at the same time, at 1.4 Ma, with the latter originating from magmatic vapor condensing into meteoric water. The subsequent phyllic assemblage followed within 100,000 yr and also was formed largely from magmatic water. This may have been the stage during which the overlying high-sulfidation ore was deposited in the advanced argillic-altered zone that caps the porphyry. It was not until the late argillic overprint—unrelated to ore—that the system was dominated by meteoric water.

Gustafson and Hunt (1975) concluded that the evolution from early K silicate to late sericitic alteration stages correlated with a transition from magmatic fluid at lithostatic pressure to a dominance of meteoric water at hydrostatic pressure. These stages are inferred to have been accompanied by a change from discontinuous brittle-ductile fractures to continuous brittle fractures, respectively, in and around the last major intrusion. Sheppard and Gustafson (1976) supported this conclusion with their interpretation of oxygen and hydrogen isotopic compositions. However, Kusakabe et al. (1990) argued that the fluid responsible for the late sericite at El Salvador reflected a magmatic signature.

Geology and Structure

The geology of the Indio Muerto area (Fig. 2), which overlies the El Salvador porphyry copper deposit (Fig. 3a), has been discussed by Gustafson and Hunt (1975) and Gustafson et al. (2001), on which we base the following summary. We have modified slightly the surface maps of these earlier workers on the basis of our field observations and study of samples (Appendix).

Late Cretaceous andesitic breccia and lavas crop out in the northern part of the area. Paleocene rhyolitic rocks, including

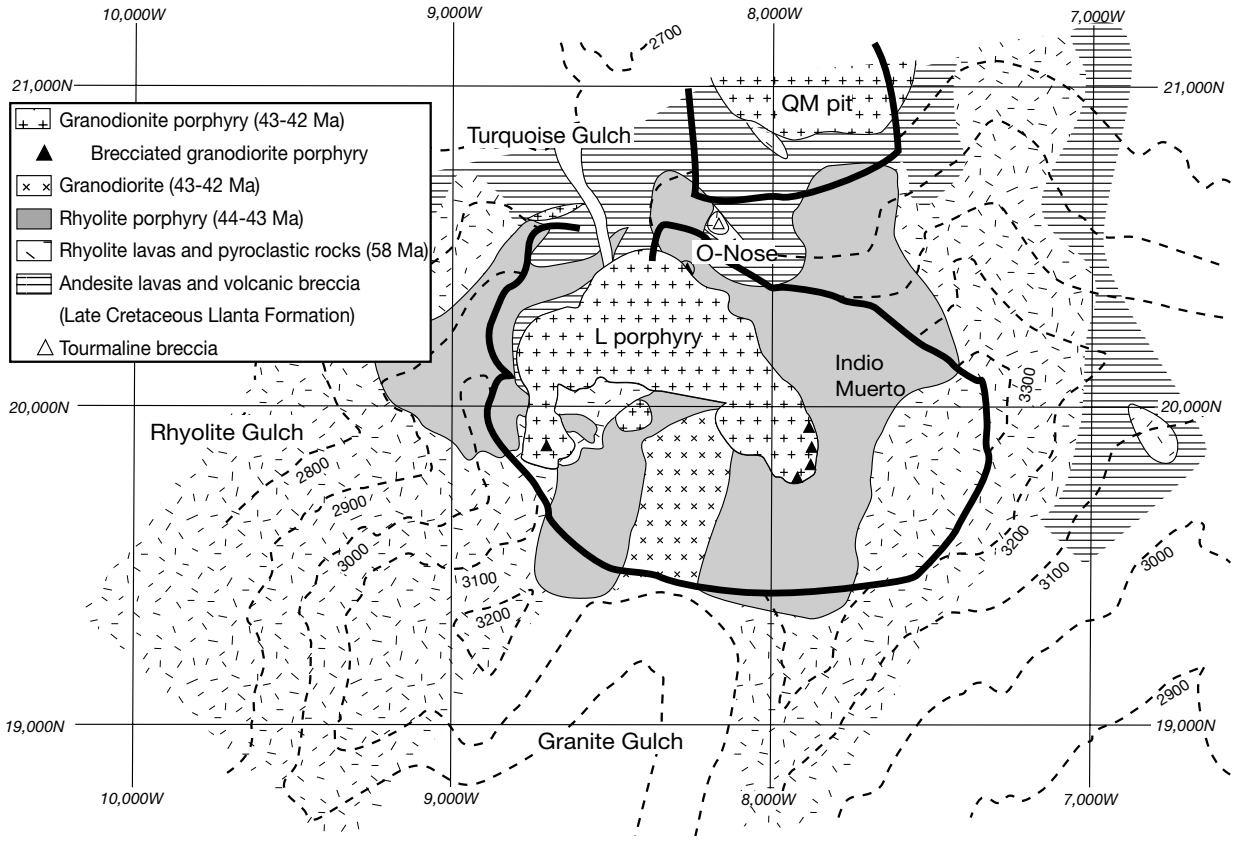

FIG. 2. Simplified geologic map of the Indio Muerto area. Rock types and contacts are taken largely from Gustafson and Hunt (1975), although the contacts were slightly modified in places on the basis of our observations. Grids are 1,000 m square, contours are 100 m. The margin of the M Gulch (QM) pit and the area of mining depression adjacent to Indio Muerto are shown by heavy lines.

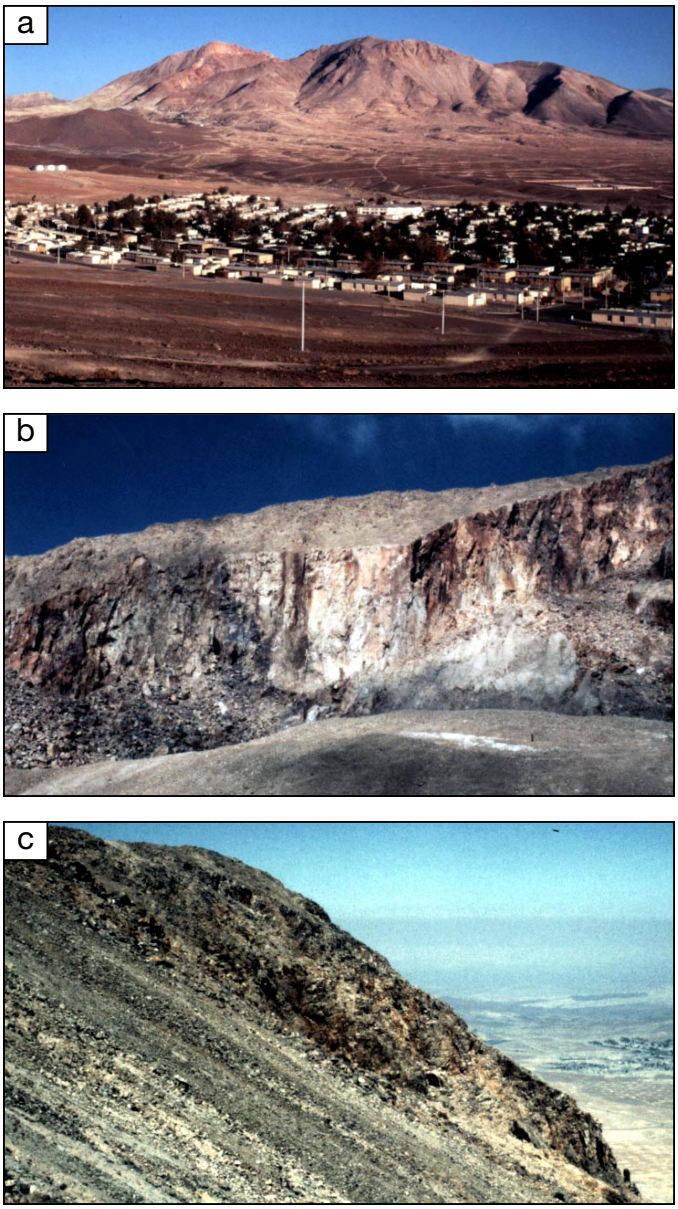

FIG. 3. Photographs of El Salvador outcrops. a. View of the Indio Muerto area, with the El Salvador mine located beneath the mountain. The left peak is the top of Indio Muerto, and the Damiana exotic copper deposit, hosted by piedmont gravel, lies between the mountain and the town of El Salvador. b. View of the cliff along O Nose, looking eastward from the central area of mining depression. The highest point is the top of Cerro Indio Muerto. The gray area to the left corresponds to an andalusite-rich patch in the muscovite-andalusite zone. The central white area corresponds to the zones of muscovite-andalusite (but poor in andalusite) and muscovite zone. The brown area to the far right at high elevation corresponds to the pyrophyllite overprint. c. The cliff consists of rhyolite lavas replaced by a dense quartz-alunite assemblage on the southwest-facing ridge between Rhyolite Gulch and Granite Gulch.

lavas, dikes, pyroclastic rocks, and epiclastic rocks, unconformably overlie and intrude the Cretaceous andesites. These rocks compose the rhyolitic dome complex that forms the main mass of Indio Muerto and has been dated at 58 to 60 Ma (Cornejo et al., 1997).

Middle Eocene rhyolite porphyry (Fig. 1) includes the fine-grained volcanic neck of Cerro Pelado and coarser dikes and sills extending from Old Camp to M Gulch — Copper Hill and Indio Muerto. It is called Quartz Porphyry by Gustafson and Hunt (1975). This magmatic sequence and associated mineralization and alteration at Cerro Pelado, Old Camp, and M Gulch, have been dated at about 44 Ma (Gustafson et al., 2001).

The granodioritic porphyry complex, dated at 43 to 41 Ma (Cornejo et al., 1997; Gustafson et al., 2001), contains multiple intrusive units and extends from Copper Hill to Granite Gulch. These units intrude the Eocene rhyolite porphyry, the Paleocene rhyolites, and the Cretaceous andesites in the Indio Muerto area (Fig. 2). Four individual centers of intrusion, brecciation, alteration, and mineralization are recognized within this complex (Gustafson et al., 2001) at M Gulch—Copper Hill, O Nose, Turquoise Gulch, and Granite Gulch in the central Indio Muerto area. The El Salvador mine, as described by Gustafson and Hunt (1975), was developed initially in the largest center, Turquoise Gulch. The present study includes samples collected at the surface over the Turquoise Gulch, O Nose, and Granite Gulch centers. The intrusive sequence in these areas includes early equigranular X porphyry, the intensely mineralized K porphyry, and the late intramineral L porphyry (Gustafson and Hunt, 1975). West-northwest–trending latite dikes that cut the granodioritic porphyry complex mark the last magmatic event in the Indio Muerto area.

Hydrothermal breccias, including some cemented by tourmaline, are present at surface. The most significant tourmaline breccia occurs at O Nose (Fig. 2), and brecciated granodiorite porphyry is located nearby. The tourmaline breccia consists of fragments of the rhyolite porphyry cemented by tourmaline and quartz. Hydrothermal breccia, the pebble dikes of H. Langerfeldt (in Gustafson and Hunt, 1975), cuts all rocks exposed at surface except latite dikes. These hydrothermal breccia dikes form a radial swarm centered on the central granodiorite porphyry (see below), and they are similar in distribution to subsurface late veins, which follow both radial and concentric patterns (Gustafson and Hunt, 1975). The breccia dikes have decimetric widths with a maximum of several meters. Their strike lengths range from a few meters to more than 1 km, and few dikes are continuous >600 m below the surface (Gustafson and Hunt, 1975). The boundaries between the breccia dikes and host rocks are normally planar and nearly vertical. Fragments are commonly rounded but angular fragments are also present, and some breccias include a flow-banded, or well-laminated, sand-size matrix.

Nature and Chronology of Alteration and Ore Minerals

Gustafson and Hunt (1975) and Gustafson and Quiroga (1995) discuss in detail the alteration, veining, and mineralization events in the main Turquoise Gulch center at El Salvador. The multiple intrusions resulted in a complexity that contributed to the observation by Gustafson and Quiroga (1995, p. 8) that "mineralization types are not necessarily time lines but rather parts of an evolving sequence which may be repeated." With this caveat in mind, we briefly summarize the evolution of this hydrothermal system.

The early alteration and mineralization stage is characterized by distinctive quartz veins (A-veins) and mainly disseminated K silicate assemblages of alkali feldspar and biotite with chalcopyrite-bornite or chalcopyrite-pyrite. The A-veins consist of granular quartz with K feldspar plus anhydrite and sulfides, lack internal symmetry, and are irregular and discontinuous. With increasing depth magnetite becomes part of all but the latest sulfide assemblages, and early biotitic veins may be the downward equivalent of the A-veins (Gustafson and Quiroga, 1995). On the periphery of the system, a propylitic assemblage of epidote, chlorite, calcite, and pyrite formed at about the same time as the central K silicate zone.

A transitional type of vein (B) formed after the last major intramineral porphyry intrusion, the L porphyry, and after the early stage of alteration and mineralization was essentially finished. These veins tend to be flat and continuous and have some internal banding, and they are associated with deposition of molybdenum. They lack K feldspar and associated alteration halos except at greater depths, where they have thick halos of K feldspar and locally andalusite. These veins cut all intrusions except for the latite dikes, although there are local occurrences of probable L porphyry cutting veins with B-type characteristics (Gustafson and Hunt, 1975).

A broad zone including andalusite surrounds the intramineral L porphyry (Fig. 4), 20 to 160 m from the porphyry contact between 2,500 and 2,750 m elevation (Gustafson and Quiroga, 1995), and it expands up to >500 m from the contact at shallow levels (Gustafson and Hunt, 1975). Andalusite appears to represent two modes of origin (Gustafson and Hunt, 1975; Hemley et al., 1980, p. 223). At depth, andalusite is associated with Na-K feldpathization of plagioclase. At shallower levels, andalusite is clearly associated with sericite (muscovite), which at least partly formed by retrograde reaction between andalusite and K feldspar (Hemley et al., 1980). Both B-veins of quartz-molybdenite and the andalusite assemblage formed during the initial cooling of the L porphyry, in the transition from feldspar-stable to feldspar-destructive and lithostatic to hydrostatic conditions; thus both can be called transitional. In addition, deep C-veins, which are cut by the later D-veins and have andalusite as well as biotite and sericite in the halos (Gustafson and Quiroga, 1995), can be considered transitional to the late D-veins with sericite halos.

A later event, characterized by abundant pyrite, was K feldspar destructive. These late D-veins crosscut B-veins and all intrusions except for the latite dikes, and they contain a variety of sulfide minerals in addition to pyrite, anhydrite, and

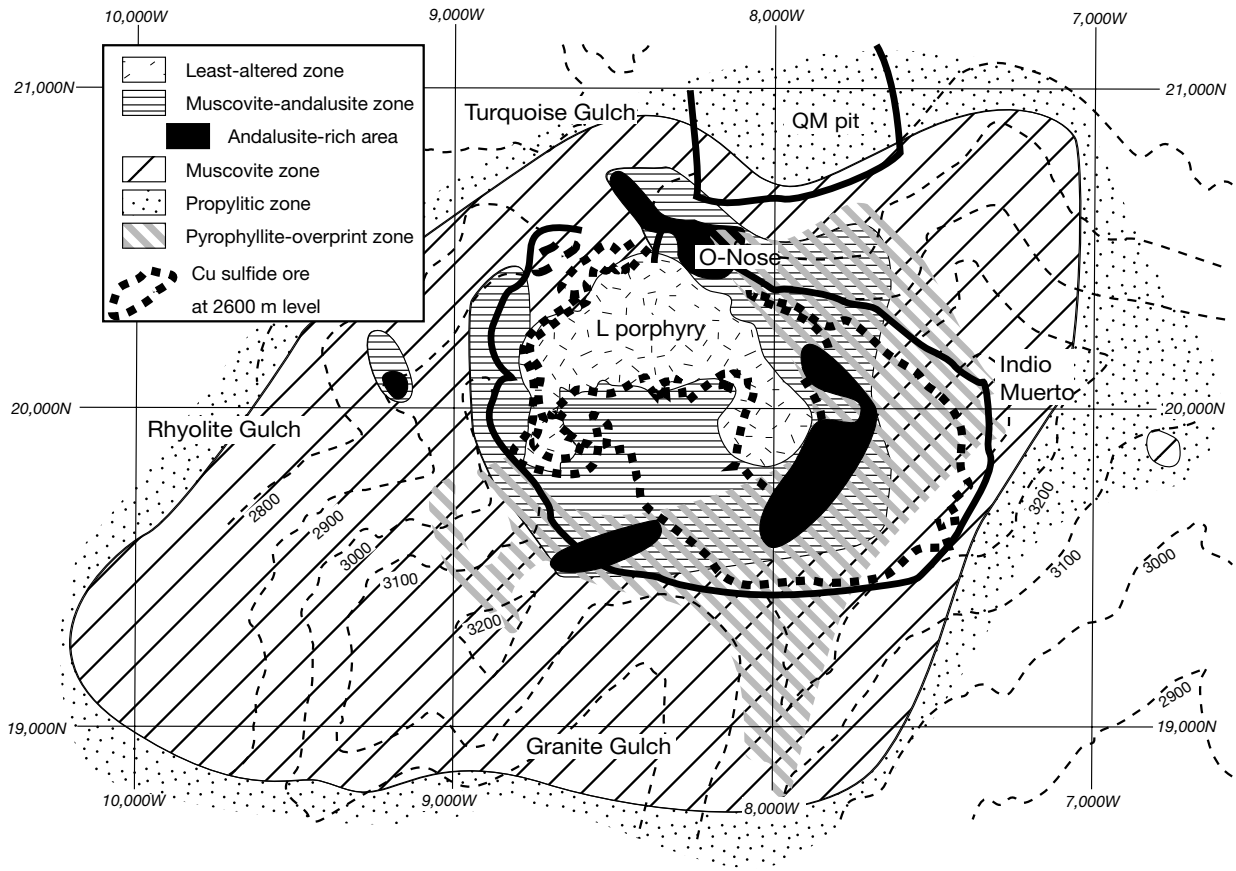

FIG. 4. Map showing the transitional to late-stage wall-rock alteration assemblages at the surface of the Indio Muerto area, on the basis of our sampling and analysis (POSAM and XRD supplemented by thin section and electron probe microanalysis study). The least-altered area corresponds generally to the central granodiorite body of late intramineral L porphyry (Fig. 2), whereas the location of the retrograde pyrophyllite zone reflects elevation. The distribution of copper sulfide ore (chalcopyrite and/or bornite) at 2,600 m elevation (from Gustafson and Quiroga, 1995) is inside the heavy broken line. Grids are 1,000 m square, contours are 100 m.

minor quartz. Alteration halos consist characteristically of sericite. Time relationships of D-veins to disseminated pyrite and veinlets with sericite plus chlorite are ambiguous, but Gustafson and Hunt (1975) suggested that the disseminated pyrite event was contemporaneous with D-vein formation. Gustafson and Hunt (1975) considered that the shallow sericite-andalusite assemblage described above is part of the late stage, although they noted that this assemblage is gradational downward to the transitional stage assemblage of andalusite-K feldspar.

The latest hydrothermal event is reflected by an advanced argillic assemblage of alunite, pyrophyllite, and diaspore. This very late stage assemblage is largely restricted to the pebble dikes around the L porphyry (Gustafson and Hunt, 1975) and zones of extension from these fractures. Although these hydrothermal breccias have the same orientation as D-veins at shallow depth, all indications are that these pebble dikes postdate D-vein formation and are thus very late (Gustafson and Hunt, 1975). Thus, the pebble dikes are essentially contemporaneous with postmineral latite dike intrusion (H. Langerfeldt, 1964, cited in Gustafson and Hunt, 1975) at 41.2 Ma (Gustafson et al., 2001).

Ore distribution and chronology

The hypogene copper ore mainly spans the contact zone between the host rocks and the central granodiorite porphyry (Turquoise Gulch center) at depths below 2,800 m elevation (Gustafson and Hunt, 1975). Gustafson and Quiroga (1995, p. 3–4) noted that most of the copper was emplaced as chalcopyrite-bornite, with K silicate alteration, in an early stage dominated by magmatic fluids (Early stage). Subsequent intrusion of the later intramineral L porphyry complex punched a large hole in the Early stage pattern. A transitional stage, in which most of the molybdenum was emplaced in B quartz veins, followed the emplacement of the L porphyry complex (Transitional stage). This event preceded the Late stage that was responsible for overprinting of pyritic, feldspar-destructive assemblages of the upper and fringe parts of the resulting pattern. Gustafson and Hunt (1975) estimated that about 75 percent of the copper was introduced during the early K silicate stage, and that at most 25 percent was deposited during late D-vein formation.

The distribution of ore at 2,600 m elevation is shown in Figure 4, from Gustafson and Quiroga (1995), who also discuss the zoning of the sulfide-ore minerals, summarized below. The inner chalcopyrite-bornite zone, locally missing because of destruction by late intrusion, has an outer halo of chalcopyrite-pyrite, which grades outward to the pyrite-only zone. Sulfide abundance decreases with depth, and a sharp downward decrease in copper values to <0.1 percent represents a barren core below the central chalcopyrite-bornite zone. The late D-veins contain pyrite and lesser but upward-increasing amounts of chalcopyrite, bornite, enargite, tennantite, sphalerite, and/or galena.

The antithetic pyrite and bornite distribution noted at depth does not hold at shallower depths, where pyrite-bornite-chalcopyrite and pyrite-bornite-digenite assemblages, with variable amounts of superimposed supergene chalcocite, exist. At surface, ore at O Nose is largely supergene chalcocite-covellite after chalcopyrite-pyrite, centered on early feldspar porphyry, although nearby at M Gulch D-veins with pyrite-bornite-digenite crop out.

Two samples of molybdenite associated with transitional stage B-veins were dated by the Re-Os method at 42.2 ± 0.19 and 42.0 ± 0.20 Ma (2σ). In addition, a five-point Re-Os isochron on the late-stage sulfides (pyrite and tennantite in D-veins) yields an age of 42.37 ± 0.45 Ma (2σ), i.e., indicating the same age for these two stages within analytical uncertainties (Watanabe et al., 1999). These dates overlap the 42 Ma timing interpreted for intrusion of the L porphyry (Gustafson et al., 2001), indicating a relatively narrow period for post-K silicate activity.

Surface Alteration Assemblages and Zonation

El Salvador is similar to many porphyry deposits, with some hypogene alteration assemblages overprinted by supergene clay minerals from the surface to depths of several hundred meters locally, depending on sulfide content and rock permeability (Gustafson and Hunt, 1975). For this reason, an attempt was made to differentiate hypogene from supergene minerals on the basis of mineral paragenesis and stable isotope studies. Measures included painstaking separation of hypogene minerals from altered feldspar-phenocryst sites only, because the phenocrysts commonly contain minerals that escaped the supergene overprint. Detailed examination of thin sections, supported by X-ray diffraction (XRD) and back-scattered electron images (petrologic and petrographic descriptions in Watanabe and Hedenquist, 1998), were conducted on one-third of the samples collected (Fig. A1). This detailed study helped to confirm the relict hydrothermal mineral assemblages and replacement textures described below.

The hydrothermal alteration zone at surface, defined by the replacement of igneous feldspars, has maximum dimensions of 3 × 2 km (Figs. 4 and A2). This zone is fringed by the propylitic alteration halo but is open to the northeast. As noted above, K silicate assemblages constitute the first alteration stage at depth. Although this early-stage assemblage was present at the elevation of the present surface, it has been obliterated by the later hydrothermal and supergene overprints. A-veins associated with this deep assemblage extend to the surface in Turquoise Gulch (Gustafson and Hunt, 1975).

There are two hydrothermal alteration events that are well preserved at the surface. We broadly correlate these two events with the transitional to late-stage and very late stage assemblages identified from subsurface studies (Gustafson and Hunt, 1975). Although the early-stage assemblage was not observed at the surface, we follow the broad four-stage terminology (early, transitional, late, and very late) developed from subsurface studies to avoid confusion.

The transitional to late-stage assemblages (andalusite and sericite) at surface occur mainly in rocks intruded by the L porphyry. The very late stage assemblage of advanced argillic minerals is associated spatially with the hydrothermal breccias and zones of pervasive quartz-alunite replacement, and with one area in particular (Fig. 5). As noted above, the very late stage assemblages at surface, partially hosted by hydrothermal pebble dikes, postdate and commonly follow the late-stage D-vein structures at depth (Gustafson and Hunt, 1975).

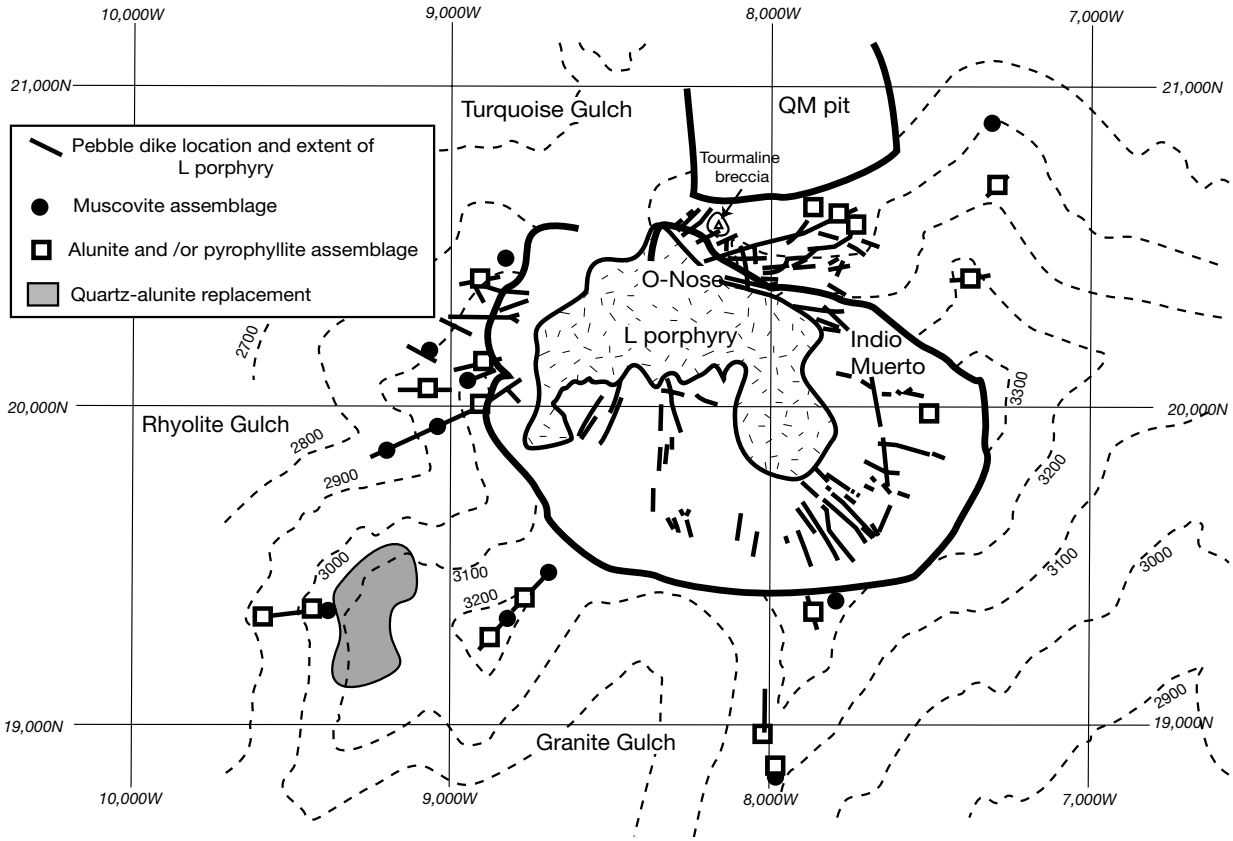

FIG. 5. Map showing the very late stage alteration assemblages associated with surface outcrops of hydrothermal pebble dikes, the latter showing a clear radial distribution around the late granodiorite L porphyry (with location shown for the 2,600 m level; Gustafson and Hunt, 1975). Grids are 1,000 m square, contours are 100 m.

Transitional to late-stage hydrothermal assemblages

We do not distinguish between transitional and late stages at surface, because shallow andalusite-bearing assemblages are "gradational, both zonally and paragenetically, with underlying andalusite and K feldspar assemblages" (Gustafson and Hunt, 1975, p. 899), even though these authors assigned the shallow andalusite-muscovite to the late stage. The muscovite-dominant assemblages at the surface are clearly late, because the pervasive sericitization and disseminated pyrite are contemporaneous with the formation of the D-veins and their sericite halos. We divide the transition to late stage into least-altered, muscovite-andalusite, and muscovite zones, which have a concentric distribution from center to margin, respectively (Fig. 4), around the L porphyry. Muscovite and quartz are ubiquitous at the surface in this central area. An overprint of pyrophyllite is recognized both in the muscovite-andalusite and muscovite zones (Fig. 4).

Least-altered zone: The distribution of the inner least-altered zone appears to correspond approximately with the location of the L porphyry (Fig. 4), although the samples available from this now-collapsed and inaccessible area are limited. Phenocrysts of plagioclase and albite in the granodiorite porphyry in this zone are preserved, although muscovite and minor tourmaline are disseminated in these phenocrysts (Watanabe and Hedenquist, 1998). Alteration halos of D-veins are quartz-sericite. Kaolinite of supergene origin (see below) commonly replaces the feldspar phenocrysts, and supergene alunite, jarosite, and kaolinite veinlets also occur in the granodiorite porphyry.

Muscovite-andalusite zone: The muscovite-andalusite zone fringes the least-altered zone (Fig. 4) and is defined by the occurrence of $2M_1$ muscovite and andalusite; euhedral diaspore is common. The host rocks of the zone include rhyolite, rhyolite porphyry, andesite, and X and K porphyries with local brecciation. Andalusite replaces hydrothermal K feldspar that formed from original plagioclase. The following observations on subsurface mineral assemblages are taken from Gustafson and Hunt (1975), unless otherwise noted.

In some specimens, andalusite makes up as much as 40 percent of the rock volume beneath surface. These andalusite-rich areas are close to and include the areas of brecciated granodiorite porphyry (Fig. 4) described by Gustafson and Hunt (1975). Silicified tourmaline breccia also occurs close to one of the andalusite-rich areas. Andalusite is common as deep as 2,500 m elevation, and occurs to depths of 1,500 m elevation, where Gustafson and Quiroga (1995) note that andalusite-muscovite is related to the contact of the L porphyry.

Andalusite coexists with muscovite at surface, but it is more commonly replaced by muscovite (Fig. 6a). Muscovite also

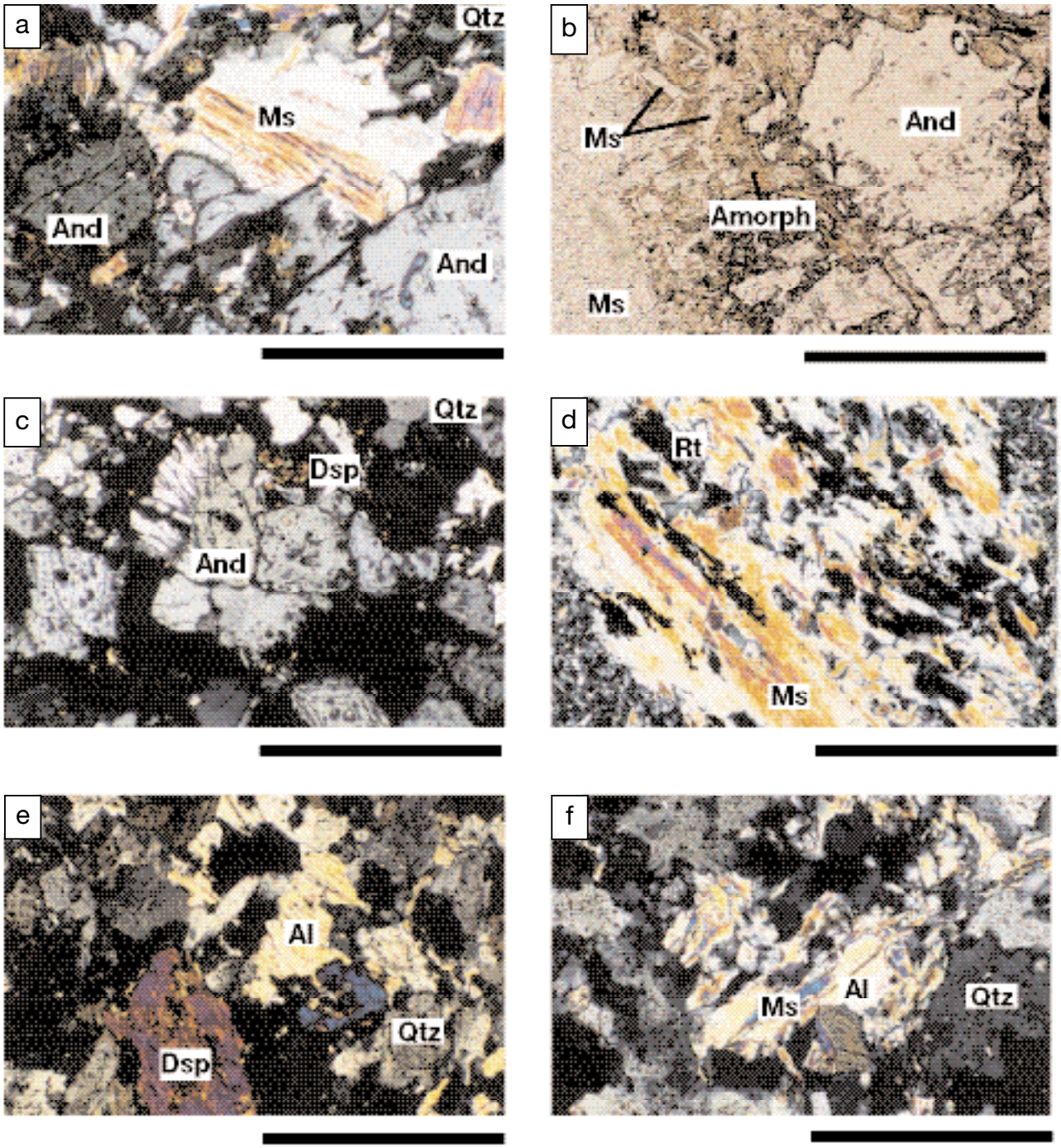

FIG. 6. Photomicrographs of altered rocks in the Indio Muerto area. a. Rhyolite porphyry in the muscovite-andalusite zone (JES-177). Margin of andalusite is replaced by muscovite (zone between andalusite and pleochroic muscovite). Bar = 0.5 mm. b. Rhyolite porphyry in the muscovite-andalusite zone (JES-188). Andalusite replaced by low refraction index amorphous material with chemical composition similar to that of andalusite. Euhedral muscovite occurs in the amorphous material. Bar = 0.5 mm. c. Rhyolite porphyry in an andalusite-rich area of the muscovite-andalusite zone (JES-195). Andalusite coexists with diaspore in phenocrysts fringed with quartz. Bar = 1 mm. d. Rhyolite porphyry in the muscovite zone (JES-125). Mafic phenocrysts are replaced by muscovite and rutile. Bar = 1 mm. e. Hydrothermal breccia affected by very late stage alteration (JES-105A). Alunite coexists with diaspore and quartz. Bar = 1 mm. f. Rhyolite lava of the quartz-alunite replacement zone (JES-159). Alunite encloses muscovite. Bar = 0.5 mm. Abbreviations: Al = alunite, Amorph = amorphous material, And = andalusite, Dsp = diaspore, Ms = muscovite, Qtz = quartz, and Rt = rutile.

has grown within an amorphous aluminum-silica material, which fringes corroded andalusite (Fig. 6b). There is abundant quartz with this assemblage, although contacts between andalusite and quartz are uncommon. Andalusite is dominant in some areas of this zone at surface (Fig. 4), where euhedral crystals occur with diaspore and quartz (Fig. 6c) and locally with corundum, as also noted in underground samples (Gustafson and Hunt, 1975). By contrast, at depth there is pseudomorphic replacement of andalusite by diaspore with muscovite rims. In some quartz-lined vugs at surface, monomineralic andalusite fills the vugs, possibly indicating local quartz-undersaturated conditions. In other cases of vug filling, andalusite and diaspore have intergrown with tourmaline, suggesting coeval generation of these three minerals.

Muscovite zone: The muscovite zone surrounds the muscovite-andalusite zone (Fig. 4). Cretaceous andesitic volcanic breccia and lava, Paleocene rhyolitic rocks, and Eocene rhyolite porphyries host this zone, which is characterized by $2M_1$ muscovite without andalusite (Fig. 6d) but with quartz. A minor amount of euhedral diaspore is present locally in this zone, replacing muscovite. Tourmaline commonly replaces muscovite, and rare disseminated dumortierite replaces tourmaline along joints near the southwestern margin of the zone. Euhedral barite occurs locally in vugs within this zone, and some portions of the zone are heavily silicified. Kaolinite and rarely paragonite occur near the outer margin of the zone. Muscovite, termed sericite by Gustafson and Hunt (1975) and others because of its fine-grained nature, is pervasive above about 2,800 m elevation and more restricted to vein halos at greater depth.

Propylitic zone: The propylitic zone (Fig. 4) fringes the muscovite zone and is distinguished from the muscovite zone by the presence of feldspars and chlorite. The Cretaceous andesitic volcanic breccia and lava and Paleocene rhyolites mainly host this zone. Illite, kaolinite, epidote, and common calcite plus rare gibbsite and stilpnomelane are also present. A sharp color demarcation, from bleached white outward to dark green, denotes the inner edge of the propylitic zone.

Pyrophyllite overprint: 2M pyrophyllite occurs in the andalusite-muscovite and muscovite zones (Figs. 3b and 4). Pyrophyllite is common at surface at higher elevations (>3,000 m) approaching the summit of Indio Muerto (Fig. 4). Its distribution is clearly a function of elevation, for example, mimicking the pattern of the ridge to the south. Pyrophyllite was also detected in samples from Tunnel 4 at 2,940 m elevation, and locally occurs below 2,700 m elevation (Gustafson and Hunt, 1975, figure 20b). Pyrophyllite-dominant rocks also occur beneath the quartz-alunite replacement zone in the southwestern part of the area (Appendix Fig. A2). Pyrophyllite commonly replaces muscovite from the outer margin of muscovite crystals and along cleavages (Fig. 7a, b), and also occurs as independent crystals (Fig. 7c). Gustafson and Hunt (1975) also noted that pyrophyllite replaces muscovite at depth. The retrograde pyrophyllite formed in a distinctly different environment from that which is part of the alunite assemblage associated with the very late stage pebble dikes (see below).

Very late stage hydrothermal assemblages

Very late stage hydrothermal assemblages at surface occur mainly in the matrix of hydrothermal breccia dikes and adjacent to the zone of quartz-alunite replacement (Fig. 3c). The hydrothermal breccias contain both muscovite and advanced argillic assemblages (Fig. 5). Advanced argillic alteration also formed a narrow halo (typically <1 m wide) around some of the pebble dikes, creating an alunite overprint on the pervasive, late-stage muscovite of the wall rock.

The muscovite assemblage includes muscovite mainly, with minor or trace amounts of alunite or pyrophyllite. The muscovite is restricted to breccia fragments in most cases, and most likely formed during pervasive sericitization that was contemporaneous with the formation of earlier D-veins, the latter subsequently intruded by the pebble dikes. The muscovite assemblage can occur alternately with advanced argillic assemblages in the same breccia dike (Fig. 5). The muscovite in the breccia matrix most likely formed by mechanical reworking of muscovite from the wall rock at depth, and for this reason should not be grouped as a very late stage event. Some pebble dikes with muscovite matrix occur near the outer margin of the muscovite zone. Elsewhere, breccia dikes with alunite halos containing aluminum-phosphate-sulfate minerals and zunyite have a muscovite matrix. It is probable that even in these situations the muscovite is reworked, rather than having an in situ origin.

The very late stage advanced argillic assemblage, as defined by Meyer and Hemley (1967), consists at El Salvador of alunite, pyrophyllite, or dickite, and is commonly associated with andalusite, diaspore, rutile, and zunyite. The occurrence of pyrophyllite is distinctly different from that associated with the retrograde alteration of muscovite, because the former is typically intergrown with alunite. Alunite exhibits compositional zoning between alunite and natroalunite (Fig. 7d). Trace aluminum-phosphate-sulfate minerals (woodhouseite and svanbergite; Fig. 7e, f) and aluminum-phosphate minerals (crandallite and florencite) also occur (Appendix Fig. A3). Zunyite is generally euhedral, although quartz and alunite locally replace portions of these crystals. Some hydrothermal breccia dikes contain few fragments of host rocks in matrices consisting of laminated and graded sand- and silt-sized alunite and quartz with kaolinite. This lamination is subhorizontal, a texture that suggests settling.

The aluminum-phosphate-sulfate and aluminum-phosphate minerals have rims of alunite and natroalunite, and they typically exhibit textures indicating partial dissolution after formation (Fig. 7e, f). These occurrences are similar to those observed in advanced argillic zones over other porphyry deposits, some hosting high-sulfidation ore deposits (Hedenquist et al., 1994; Arribas et al., 1995; Losada-Calderón and McPhail, 1996). The mineral cores are generally rich in Ba, Ca, and Sr as well as rare earth elements (REEs) such as Ce, Nd, and La. Some supergene alunite (see below) and jarosite contain trace amounts of aluminum-phosphate minerals.

A cliff outcrop of quartz-alunite replacement of flow-banded rhyolite occurs between Rhyolite Gulch and Granite Gulch in the southwestern part of the Indio Muerto area (Fig. 5). This massive replacement occurs at an elevation of about 3,100 m, is 80 m thick, and extends over an area of about 500 × 300 m (Fig. 3c). The host rock consists of flat to steeply flow-banded rhyolite lavas altered pervasively to quartz-alunite. There is an underlying hydrothermal breccia approximately 3 m thick that crops out above about 2,900 m elevation

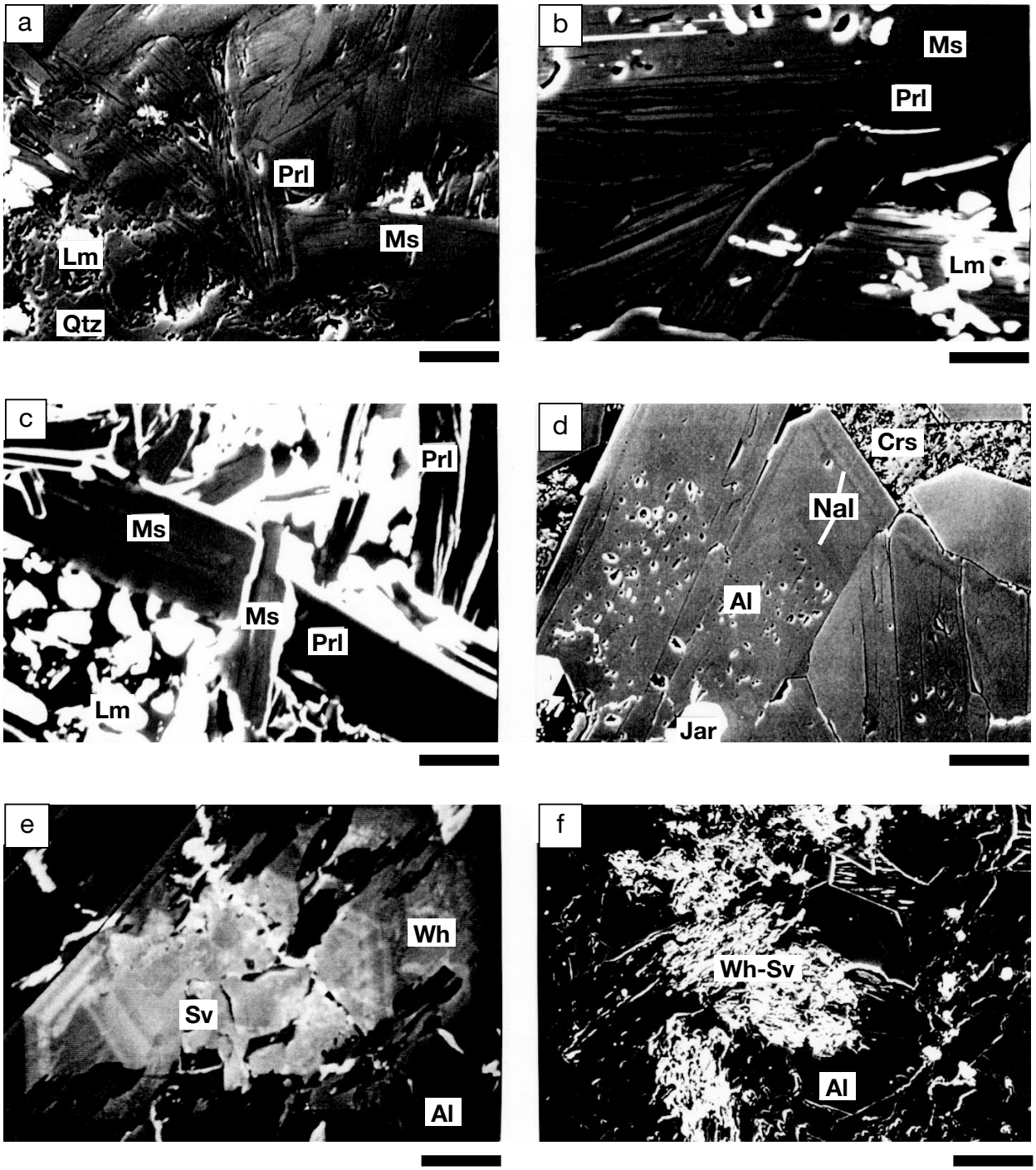

FIG. 7. Back-scattered electron images of alteration minerals. a. Rhyolite porphyry in the muscovite-andalusite zone (JES-126). Pyrophyllite (darker color) occurs at the margins of muscovite crystals (lighter color). Bar = 40 μm b. Rhyolite lava in the muscovite zone (ES-7260). Pyrophyllite occurs along cleavages of muscovite. Bar = 10 μm. c. Rhyolite lava in the muscovite zone (ES-7260). Pyrophyllite occurs as independent crystals coexisting with muscovite crystals. Bar = 10 μm. d. Hydrothermal breccia in the muscovite zone (JES-105A). Euhedral alunite crystals exhibit alternating bands of alunite (lighter color) and natroalunite (darker color). Bar = 40 μm. e. Hydrothermal breccia in the muscovite zone (ES-6573). Euhedral alunite crystals include svanbergite enclosed in woodhouseite. The svanbergite is rich in Ce, Ba, and Ca. Bar = 10μm. f. Hydrothermal breccia in the muscovite zone (JES-105A). Alunite crystals include woodhouseite-svanbergite solid solution that exhibits dissolution texture. The solid solution is rich in REEs such as Ce, La, and Nd. Bar = 60 μm. Abbreviations of minerals: Al = alunite, Crs = cristobalite, Jar = jarosite, Lm = limonite, Ms = muscovite, Nal = natroalunite, Prl = pyrophyllite, Qtz = quartz, Sv = svanbergite, and Wh = woodhouseite.

(Fig. 5). This breccia dike may be the feeder to the zone of replacement, because there is no evidence of the breccia dike cutting the replaced rock. The dense quartz-alunite replacement shows a sharp lower contact with late-stage pervasive muscovite, whereas there is a gradual overprinting of this muscovite by alunite laterally.

Alteration minerals in the replacement zone consist dominantly of quartz and alunite with minor remnant muscovite (Fig. 6f). The alunite is mostly potassium-rich and is generally coarser (up to 10 mm) than that in the hydrothermal breccias. Alunite replaces muscovite completely at the center of the massive replacement body but muscovite remains at its margin. Aluminum-phosphate-sulfate minerals were not detected and are apparently restricted to the breccia dikes.

Isotopic Composition of Minerals

Mineral separates were prepared from samples collected from surface, whereas supergene kaolinite was collected from shallow depths in surface-collared drill holes (locations shown in Fig. A1).

O and H isotope compositions of silicate minerals

The O and H isotope composition of muscovite, pyrophyllite, dickite, and supergene kaolinite were analyzed after careful hand picking, separation, and purification (Appendix). Hypogene samples for which X-ray diffraction analysis indicated more than a trace (>5%) of kaolinite were discarded.

The results for each sample, including the water content of samples analyzed for δD, are listed in Table A1, and the results are plotted on an isotope diagram (Fig. 8a). The muscovite samples form a relatively tight group. Muscovite from JES-119, although displaced from other muscovite samples with the lightest δD value, has an XRD pattern indicating that it is pure. The supergene kaolinite samples have compositions that lie near the kaolinite line. Sheppard and Gustafson (1976) analyzed three samples of muscovite collected from underground, plus three samples of supergene kaolinite (plotted as M and K, respectively). Most of their samples are similar in composition to ours. One of their samples identified as kaolinite, from a D-vein halo at 2,400 m elevation, plots relatively near one of our very late stage hydrothermal dickite samples.

O, H, and S isotope compositions of alunite

Alunite samples were prepared for O (and some for S) isotope analysis by first dissolving the alunite in NaOH (Appendix). After dissolution, the residue was examined by XRD, and some samples from breccias were found to contain resistant aluminum-phosphate minerals (Table A1) that existed as cores of the laboratory-dissolved sulfate minerals.

The S isotope composition of alunite ranges from 9.6 to 18.8 per mil δ^{34}S (Table A1). The samples from the quartz-alunite replacement outcrop have a narrower range of 14.4 to 16.7 per mil. One sample (JES-211) had a core and rim of alunite that were similar in composition (18.4‰ and 18.8‰). δ^{34}S analyses were also made on the NaOH-prepared barite precipitate, unaffected by traces of sulfide minerals. These analyses agree well with the results obtained by direct preparation of alunite by KIBA dissolution (Table A1). Thus, the relatively light δ^{34}S values of some of the hypogene alunites are not the result of incorporation of sulfide minerals, consistent with XRD evidence of no sulfide contamination.

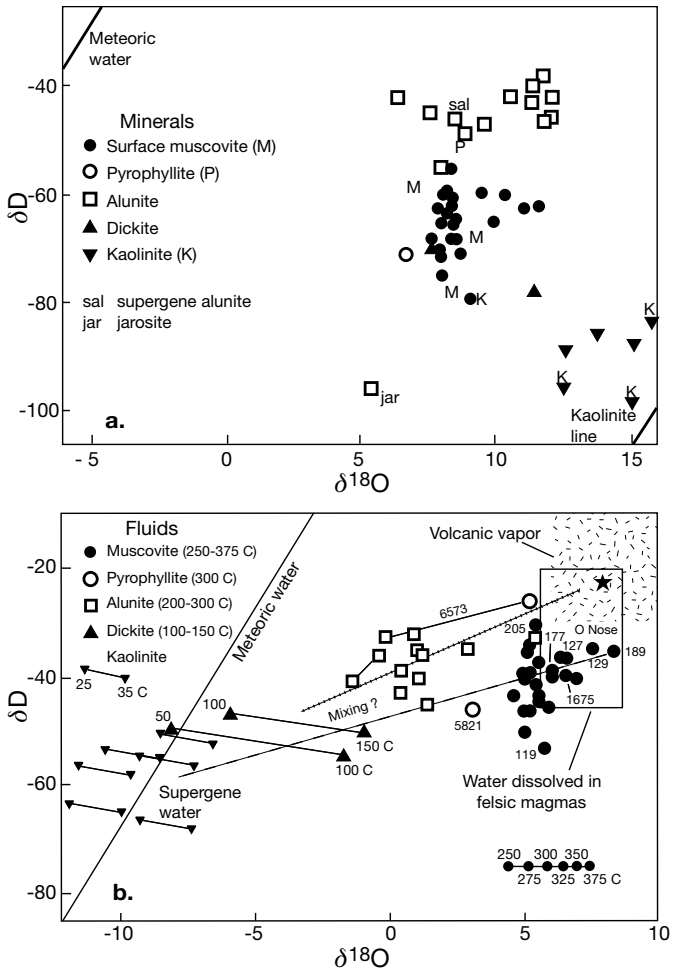

FIG. 8. a. O and H isotope composition of silicate minerals and alunite from surface samples at El Salvador, shown as symbols. Letters denote the composition of minerals reported by Sheppard and Gustafson (1976); M = muscovite, P = pyrophyllite, and K = kaolinite. There is good agreement between the two studies for similar minerals. b. O and H isotope compositions of hydrothermal fluids, calculated from mineral analyses using temperatures (Table 1) indicated from the mineral assemblage for each sample (Figs. A2 and A3). Fractionation factors listed in Hedenquist et al. (1998); the fractionation factors for muscovite were used for the pyrophyllite calculation. The range of isotopic composition of typical volcanic vapor is from Giggenbach (1992a), and for water dissolved in felsic magma from Taylor (1992). Hydrothermal liquid responsible for forming the late-stage muscovite appears to have been dominantly of magmatic origin, whereas pyrophyllite replacing muscovite indicates a component of meteoric water, the latter similar in composition to that which formed the posthydrothermal supergene kaolinite. By contrast, very late stage breccia dikes and the quartz-alunite replacement contain alunite and pyrophyllite that indicate formation from volcanic vapor condensed by meteoric water, with very late stage dickite formed from relatively cool, meteoric-water–dominant solutions.

One group of alunite samples range from –4.7 to 1.4 per mil δ^{34}S, and the two pyrites separated from the NaOH-treated residue of these samples have values of –3.2 and –5.2 per mil. The similarity of sulfate and sulfide values indicates the alunite formed at low temperature, most likely under supergene conditions. As noted above, the aluminum-phosphate minerals in the residue of supergene alunite samples indicate that

some supergene alunite formed as a replacement of hypogene alunite with hypogene aluminum-phosphate cores. Therefore, even though the hypogene samples are sulfide free, isotopically light S from partial supergene replacement may be present. This would explain the low $\delta^{34}S$ values for some alunite samples from breccia dikes, consistent with partial replacement of hypogene alunite by supergene alunite. Such a mixture may also account for the difficulty of dating alunite samples from El Salvador (Gustafson et al., 2001).

The alunite samples that were analyzed for both $\delta^{18}O$ and δD are also plotted on Fig. 8a. With the exception of two samples with light $\delta^{18}O$ values, the data trend has a positive slope. The supergene alunite sample lies close to the trend for hypogene alunite, i.e., supergene replacement appears to affect only the S isotope value and not $\delta^{18}O$ or δD. By contrast, the supergene jarosite has an exceptionally light δD value (Fig. 8a). Both supergene sulfate samples had crandallite, an aluminum-phosphate mineral, in their NaOH-treated residue. Two other occurrences of aluminum-phosphate minerals were found in samples of hypogene alunites from hydrothermal breccias near the quartz-alunite outcrop, one crandallite and the other florencite, a REE-rich variety (Table A1).

Interpretation and Discussion

Transitional to late-stage assemblages

The zoning of the transitional to late-stage assemblages suggests that the granodiorite L porphyry at the center of the Indio Muerto area focused the flow of hydrothermal solutions during this late intramineral period. This conclusion is consistent with arguments by Gustafson and Hunt (1975), who also noted that K feldspar-andalusite grades upward to andalusite-muscovite. The correlation of the locations of andalusite-rich zones and brecciation of the granodiorite porphyry also suggest that there was more than one hydrothermal center in the granodiorite porphyry, and alteration is associated with hydrothermal brecciation at these centers (cf. Gustafson et al., 2001). The concentric zoning of the transitional to late-stage assemblages at Indio Muerto may have formed by coalescence of these smaller centers of hydrothermal minerals, themselves concentric to the late porphyry intrusion (Fig. 4). The lack of a strong hydrothermal imprint on much of the central L porphyry, the least-altered zone, is consistent with hydrothermal fluid ascending from greater depths along the margin of this late intramineral porphyry, such that only the crystallized margin was altered extensively.

The temperature variation of the hydrothermal solution can be estimated from mineral assemblages, using constraints from experimental studies (Figs. 9 and 10; Hemley, 1959; Hemley et al., 1980; Sverjensky et al., 1991; Frank et al., 1998) and active-system studies (Reyes, 1990; Reyes et al., 1993). Pressure affects the temperature stability of these assemblages to some degree. At the few-kilometer paleodepth represented by the present surface, the pressure was somewhere between lithostatic and hydrostatic (i.e., saturated vapor pressure) during the transitional to late stages (Gustafson and Hunt, 1975). For example, at a pressure of 1 kbar, which is equivalent to lithostatic pressure at about 3 km depth, the equilibrium temperature of a given assemblage is only slightly higher than at hydrostatic pressure (Fig. 10). Furthermore, the relative temperature differences of these assemblages do not change with pressure.

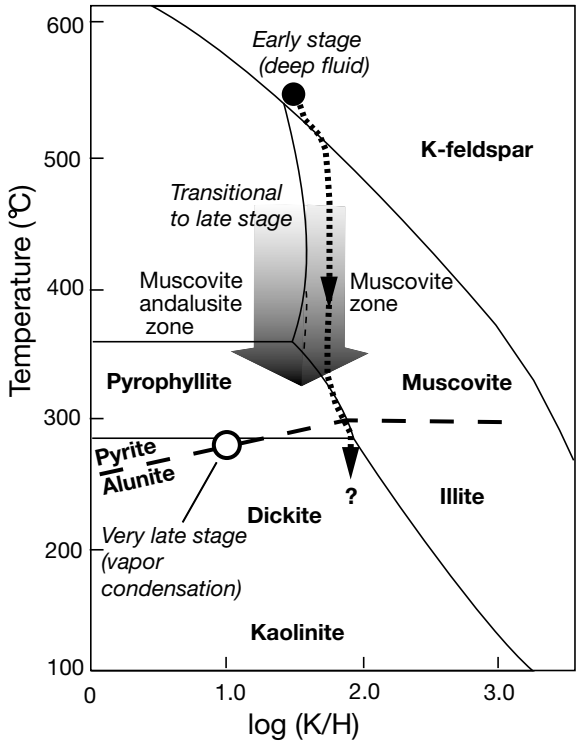

FIG. 9. The stability of Al silicate minerals as a function of K/H mole ratios vs. temperature, at quartz saturation and 1 kbar (from Hemley, 1959; Sverjensky et al., 1991); there is little difference at lower pressure. Some andalusite assemblages at El Salvador appear to be quartz-undersaturated (see text). The evolutionary path deduced for transitional to late-stage fluid at Indio Muerto is indicated, with the cooling path either andalusite-muscovite or muscovite-only stable. The muscovite-only stable path is shown by the short dotted line, with cooling causing retrograde pyrophyllite to form. The very late stage fluid formed by condensation of volcanic vapor to create an acidic fluid, distinct in composition from the transitional to late-stage fluid. The position of the pyrite-alunite coexistence line was estimated from thermodynamic data and relationships in active systems (Giggenbach, 1992b).

The change of mineral assemblage from K feldspar with andalusite at depth (Gustafson and Hunt, 1975) to andalusite with muscovite at elevations corresponding to the present surface indicates a cooling of the hydrothermal fluid during ascent (Hemley, 1959; Fig. 9). The scarcity of muscovite in the core areas of the muscovite-andalusite zone and the absence of andalusite in the muscovite zone indicate that the K/H mole ratio of the hydrothermal solution increased towards the margin of the system. This outward change was possibly caused by a lower fluid-to-host rock ratio, i.e., greater neutralizing capacity (cf. Frank et al., 1998). The textures indicating that andalusite was replaced by muscovite in the muscovite-andalusite zone suggest that the hydrothermal solution decreased in temperature, and/or the K/H mole ratio may have increased (Fig. 9) with time.

An assemblage of corundum, andalusite, and diaspore indicates a temperature of >370° to 400°C (Fig. 10; summarized in Table 1). The assemblage of andalusite and muscovite (±

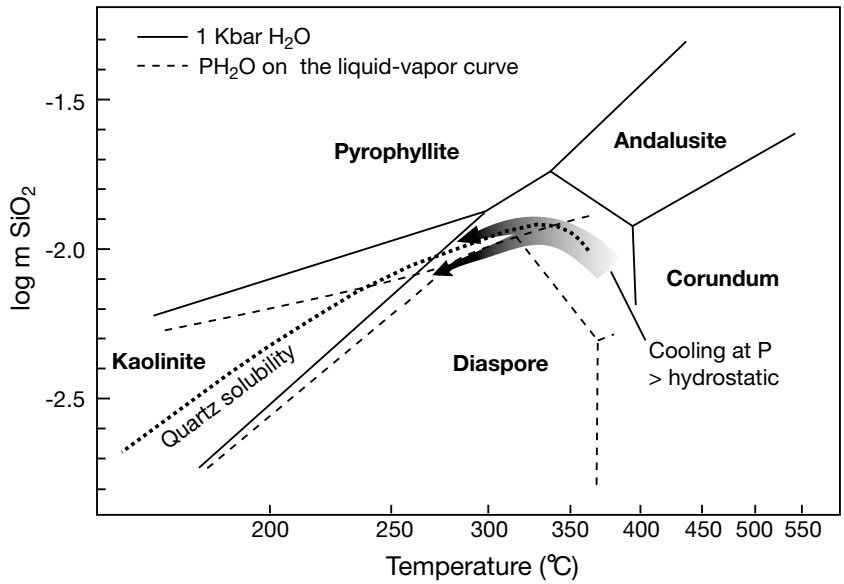

FIG. 10. Stability relationships in the system Al_2O_3-SiO_2-H_2O at 1 kbar H_2O pressure and along the liquid-vapor curve (from Hemley et al., 1980). The possible evolutionary path of transitional to late-stage solution at Indio Muerto is indicated. The fluid evolved along the path from the triple junction of corundum, andalusite, and diaspore to the pyrophyllite-diaspore univariant, through to the junction among andalusite, diaspore, and pyrophyllite. The fluid may have been locally quartz-undersaturated, i.e., during andalusite formation and while pyrophyllite was altering muscovite (see text). The pressure during the transition to late stages would have been between 1 kbar (solid lines) and hydrostatic (broken lines), with the maximum pressure at the level of the present surface likely <500 b (Gustafson and Hunt, 1975; Gustafson and Quiroga, 1995). The very late stage fluid may have entered kaolinite stability along the pyrophyllite-diaspore univariant under hydrostatic conditions.

diaspore) at quartz saturation suggests a slightly lower temperature, perhaps 360° to 375°C (Fig. 9). Although andalusite does not in all cases coexist with muscovite, and it is commonly replaced by muscovite, the presence of euhedral diaspore coexisting with andalusite suggests a temperature >310°C. The solution responsible for the muscovite zone (± diaspore) had a temperature lower than that of the muscovite-andalusite zone, whereas the temperature was higher than that of pyrophyllite-muscovite equilibrium at quartz saturation (Fig. 9). The pyrophyllite-bearing assemblage of the later overprint indicates a temperature of 280° to 360°C, and the presence or absence of andalusite in this pyrophyllite-bearing assemblage indicates a relatively higher or lower temperature in this range, respectively, at least during andalusite formation, or a lower or higher K/H mole ratio, respectively. The temperature of the hydrothermal solution at the outer margin of the muscovite zone (lacking diaspore) was most likely <280°C, as indicated by the absence of pyrophyllite (Fig. 4). However, we must keep in mind the possibly later timing of the pyrophyllite relative to the rest of the transitional to late-stage assemblages at the present surface.

TABLE 1. Temperatures Deduced for Various Mineral Assemblages and Used in Calculations

Assemblage	Temperature of assemblage (°C)	Temperature used in calculation
Andalusite-corundum-muscovite	>370–400	400
Andalusite-muscovite ± diaspore	310–400	375
Muscovite-diaspore	260–370	325
Diaspore-pyrophyllite-muscovite	290–360	300
Pyrophyllite	280–360	300
Muscovite-pyrophyllite	280–360	275
Muscovite	<280	250
Dickite	<100–200 (<270)	50, 100, 150
Alunite-APS-diaspore	<320	300
Alunite-APS	250	250
Alunite	200	200
Supergene kaolinite	10–40	25, 35

For higher temperature assemblages, pressure is assumed to vary between 1 kbar and saturated vapor pressure, whereas at lower temperature (<300°–350°C), pressure is assumed to be hydrostatic, i.e., saturated vapor pressure; note that for isotope calculations and all subsequent interpretations, the relative temperature difference between assemblages is more critical than the absolute temperature of equilibration

Absence of kaolinite-group minerals (dickite, nacrite, and kaolinite) and coexistence of pyrophyllite and diaspore during the late stage suggests that the temperature of this solution did not cool to reach the kaolinite-stable field in the core of the system at the level exposed (Figs. 9 and 10). However, the absence of pyrophyllite and presence of hypogene (?) kaolinite on the outer margin of the muscovite zone and in the propylitic zone indicate that the hydrothermal solution had a lower temperature (and higher K/H mole ratio, possibly higher pH) than that in the inner part of the muscovite zone.

The later overprint of muscovite ± andalusite by pyrophyllite at higher elevations during the late stage indicates that the temperature of the solution decreased in the muscovite-andalusite and muscovite zones (Fig. 9). Although this later, lower temperature solution was overall ascendant, as indicated by its isotopic composition, in some cases it may have also flowed laterally or even descended along structures on the margin of the system. Such flow may account for the

muscovite-pyrophyllite assemblage in Tunnel 4 (at 2,940 m elevation) and at greater depths (Gustafson and Hunt, 1975).

Very late stage assemblages

As indicated by the isotopic composition of the alunite (see below), the very late stage acidic fluid was generated by condensation of magmatic vapor containing acidic volatiles. The preservation of at least a portion of a possibly extensive quartz-alunite zone indicates that this acidic hypogene fluid continued to ascend along the hydrothermal breccia zones after their formation, flowing into the wall rocks in zones of lateral permeability in the flow-banded rhyolites.

The temperature indicated by the advanced argillic assemblages (Fig. 5) can be estimated from phase relations (Fig. 10), i.e., andalusite-diaspore-pyrophyllite (320°C), diaspore-pyrophyllite (270°–320°C), and dickite-dominant (<270°C). Alunite occurs in most assemblages as a major constituent. When aluminum-phosphate-sulfate minerals occur with alunite, and diaspore is present, we assign a temperature of alunite formation of 300°C; for alunite plus aluminum-phosphate-sulfate minerals only, 250°C, and for alunite only, 200°C (Table 1). This relative decrease in temperature is based on similar assemblages at Lepanto that were calibrated with S isotope data (Hedenquist et al., 1998).

Aluminum-phosphate-sulfate minerals form when a highly reactive fluid dissolves primary apatite to release phosphate and other components to solution (Stoffregen and Alpers, 1987), hence their hypogene origin. The temperature during the transitional to late stages was about 360° to 290°C, whereas during the very late stage temperature was largely <300°C. The lower temperature resulted in the fluid becoming more reactive due to dissociation of HCl and H_2SO_4. This caused dissolution of the aluminum-phosphate-sulfate minerals and their replacement by alunite, followed by the appearance of a dickite-dominant assemblage in the hydrothermal breccias. The absence of aluminum-phosphate-sulfate minerals in the quartz-alunite replacement zone may also support this pattern of pH decrease with decrease of temperature, from the feeder breccia to the replacement zone. An aluminum-phosphate-sulfate mineral–alunite assemblage appears to occur at a higher temperature and/or closer to the magmatic source, than alunite without aluminum-phosphate-sulfate minerals (Hedenquist et al., 1998).

The $\delta^{34}S$ composition of hypogene alunite collected from the surface ranges from 10 to 18 per mil. None of these samples was found to coexist with a sulfide mineral, although this finding may have been due to the effects of supergene oxidation of sulfides. Field and Gustafson (1976) report an average $\delta^{34}S$ composition of –2 ± 1 per mil for 10 pyrite samples associated with sericitic, propylitic, and advanced argillic assemblages. Our two pyrite samples from breccias with supergene alunite have values of –3 and –5 per mil. Assuming a minimum sulfide value of about –5 per mil $\delta^{34}S$, the equilibrium S isotope temperatures (Ohmoto and Goldhaber, 1997) for alunite formation range from 375° to 250°C. By contrast, using the –2 per mil average pyrite value for samples associated with the transitional stage, the temperature range would be 450° to 300°C. These calculated S isotope temperatures are higher than and inconsistent with the 300° to 200°C values we estimate from mineral assemblage information.

This inconsistency in temperature estimates may be due to lack of equilibrium between hypogene sulfate and sulfide minerals, or we may not have a representative $\delta^{34}S$ value of the sulfide in equilibrium with the alunite. Alternatively, many of the apparently hypogene alunite samples may be incompletely altered to supergene alunite, resulting in a bulk alunite sample with an isotopic composition intermediate between the hypogene and supergene end-member values. This conclusion is supported by the presence of aluminum-phosphate-sulfate and aluminum-phosphate minerals within supergene alunites (i.e., with $\delta^{34}S$ values <0‰), indicating that in some cases supergene alunite replaced hypogene alunite. If this latter explanation is true, then the actual range of hypogene $\delta^{34}S$ values may lie between 14.4 per mil (the lightest value from the dense replacement alunite) and 18.8 per mil (the heaviest value found). Using a –2 per mil sulfide value, this range would indicate equilibrium temperatures of 375° to 300°C, closer to the temperature estimated from mineral assemblage constraints. Using the –5 per mil sulfide value would result in a range about 50°C lower, in close agreement with the temperature estimates from mineral assemblages.

Isotopic composition of hydrothermal fluid

The information on mineral assemblages (Figs. 4 and 5) was used in conjunction with experimental results (Figs. 9 and 10) to estimate paleotemperatures (Table A1). The temperature assigned to each assemblage (Table 1) then allowed calculation of the isotopic composition of associated hydrothermal fluid for each sample on the basis of its mineral assemblage (Figs. A2 and A3; Table A1), using fractionation factors compiled by Hedenquist et al. (1998; their appendix table 1).

Transitional to late-stage alteration assemblages: Five muscovite-bearing assemblages were observed in our samples collected from the surface; andalusite-corundum-muscovite occurs only at depth. These five assemblages are deduced to have formed at temperatures ranging from 375° to 250°C (Table 1). On the basis of these temperature estimates, the calculated fluid responsible for forming the muscovite at the present surface had a relatively narrow range of isotopic composition, 6.5 ± 1.5 per mil $\delta^{18}O$ and –40 ± 10 per mil δD (Fig. 8b), despite the 24 pure mineral separates coming from an area of >4 km^2.

Two subtle groupings of samples may emerge when one considers mineral assemblage and geographic distribution. Samples with the highest temperature assemblage, andalusite-muscovite-diaspore, all occur within a radius of 500 m, with a center near O Nose. Five of six of these samples have the heaviest calculated $\delta^{18}O$ and δD fluid values (JES 127, 129, 177, 189, and 1675) and, along with three other samples in this northern area, form one group with an end member labeled O Nose on Figure 8b. The rest of the samples have a very narrow range of $\delta^{18}O$ values, 5.5 ± 0.5 per mil, whereas they have a δD range in excess of 20 per mil, with the sample having the lowest δD value (JES 119) coming from the southwest at 3,200 m elevation (Fig. A1).

Compared with the average fluid in equilibrium with muscovite, one sample of late-stage pyrophyllite (retrograde after muscovite) indicates an isotopically lighter fluid composition (Fig. 8b). The trend of $\delta^{18}O$ and δD fluid composition, from

muscovite to pyrophyllite, is consistent with dilution of the isotopically heaviest fluid (JES 129 and 189) by meteoric water, as noted in some other porphyry deposits (Hedenquist et al., 1998). Composition of the meteoric water is assumed to be similar to that indicated by the supergene kaolinite samples (see below), and that similarity suggests a progressive but nevertheless slight encroachment of meteoric water as the temperature waned.

The isotopic compositions of El Salvador muscovite indicate a relatively homogenous fluid formed the phyllic assemblage (Fig. 8b). Thus, regardless of the origin of this fluid, we conclude that the isotopic composition of phyllic minerals would not be useful at El Salvador to target an intrusive center during exploration. The zoning is very subtle and is strongly dependent on the estimated equilibration temperature. If we assume that the fluid calculated for samples 129 and 189 is essentially end-member magmatic in origin, as its composition suggests, there was no more than 10 to 20 percent meteoric water involved in producing the other surface muscovite samples at El Salvador.

This calculated composition of the fluid responsible for the phyllic stage is similar to that determined for other porphyry copper deposits (Hedenquist and Richards, 1998). For example, the fluid that formed muscovite (illite) in the mineralized core of the Far Southeast porphyry deposit had an average composition of 5.5 δ^{18}O and –40 per mil δD, consistent with a magmatic origin (Hedenquist et al., 1998). In comparison, illite from the marginal phyllic zone at Far Southeast, only 500 m away from the core, had a composition of 2 and –50 per mil, indicating a 30 percent component of local meteoric water on the margin of this deposit. Therefore, the results for the El Salvador phyllic assemblage are surprising in their homogeneity over a much larger area.

Very late stage alteration assemblages: Hypogene alunite forms where magmatic vapor is absorbed by meteoric water before it can discharge to the surface from a volcanic fumarole. The composition of local meteoric water at the time of this hydrothermal activity, 41 Ma, is unknown. However, its composition can be estimated from supergene clays, even though they formed after hydrothermal activity ceased.

Supergene processes occurred at a variety of times, typically <36 Ma (Mote et al., 2001). We assume that our supergene kaolinite samples formed from meteoric water that was similar in composition to that during hydrothermal activity. The supergene kaolinite samples have calculated water values that cross the meteoric water line if a 25° to 35°C range of temperature is used for calculation (Fig. 8b). This temperature range is reasonable considering the exothermic reaction that occurs during sulfide oxidation which led to formation of the supergene kaolinite. The variation of calculated meteoric water composition is ~15 per mil δD, suggesting samples may have formed at somewhat different times and elevations. A mixing line (Fig. 8b; dotted line) between this general paleometeoric water composition and an average volcanic vapor (Giggenbach, 1992a) provides one reference for interpretation of the alunite data, since studies elsewhere have demonstrated that quartz-alunite alteration originates from magmatic vapor absorbed by local groundwater (Arribas, 1995).

We calculated the composition of the very late stage fluid responsible for forming the hypogene alunite by using the temperatures estimated from the associated mineral assemblage (Table 1). The fluid compositions range from 5 per mil and –30 per mil to –1 per mil and –40 per mil δ^{18}O and δD, respectively (Fig. 8b, boxes). This range in composition agrees with the trend predicted for magmatic vapor absorbed by local groundwater (dotted line). Therefore, it appears that the very late stage advanced argillic alunite assemblage formed by groundwater absorption of magmatic vapor during discharge along the hydrothermal breccia dikes. We recalculated the fluid composition in equilibrium with the sample of pyrophyllite from a breccia dike (ES 6573), analyzed by Sheppard and Gustafson (1976), using a mineral assemblage temperature of 300°C for the assemblage alunite–aluminum-phosphate-sulfate minerals–diaspore–pyrophyllite. We also analyzed alunite from the same sample, shown with a tie line to the pyrophyllite. The compositions of fluid that formed this alunite and pyrophyllite are also consistent with the magmatic water and meteoric water mixing trend (Fig. 8b).

We analyzed two dickite samples, one replacing rhyolite porphyry (JES 135) and the other from breccia of Quartz Porphyry (JES 212). Using temperatures of 100° to 150°C, the calculated fluid compositions are close to the mixing trend between muscovite and meteoric water, whereas at about 50° to 100°C, the compositions would plot near the mixing trend of alunite and meteoric water. These compositions suggest that dickite formed during the waning and relatively cool portion of the late to very late stage.

Isotopic zoning

There is no systematic spatial zonation in isotopic composition or temperature of the El Salvador alunite samples. This is different from the situation at Far Southeast–Lepanto, where the alunite records a simple trend of increasing meteoric water component with increasing distance from the porphyry, from 10 to 50 percent as distance from the porphyry increases to 3 km. This clear zonation at Far Southeast was likely caused by the focused nature of the discharge. Unidirectional outflow occurred over a distance of >4 km along the Lepanto fault at the basement unconformity. By contrast, the radial dikes at El Salvador are all in a proximal position relative to the late intramineral granodiorite porphyry (Fig. 5). In addition, an extensive zone of advanced argillic alteration is preserved above the phyllic alteration zone at the Far Southeast deposit, whereas the phyllic alteration zone is exposed at the surface at El Salvador. The relative levels of intrusion also suggest greater erosion and deeper exposure at El Salvador. For this reason, much of the advanced argillic replacement at El Salvador has likely been eroded.

The lack of any simple isotopic zonation for either muscovite or alunite may also be due to the relative complexity of the El Salvador hydrothermal system, caused by the multiple episodes of intrusion (Gustafson and Hunt, 1975), and a possibly long-lived system (Gustafson et al., 2001). This complexity of intrusion and alteration may have homogenized preexisting isotopic patterns, although there is very little isotopic variation in the phyllic assemblage in any case (including underground samples at >500 m depth; J. Hedenquist, unpub. data). Dating of pure samples of surface alteration minerals, although desirable, may not resolve this situation, since the analytical error at 42 Ma might be too great to

indicate clearly a progressive age of multiple phases of either muscovite or alunite.

Some workers have argued that an isotopically heavy fluid, similar to the one we determined for phyllic alteration at El Salvador, can originate by an O isotope shift of meteoric water (Taylor, 1974; Sheppard and Gustafson, 1976). However, we believe that this fluid was magmatic in origin, following the arguments made by Hedenquist and Richards (1998) and Hedenquist et al. (1998). The waters responsible for formation of phyllic assemblages in porphyry deposits have compositions far from local meteoric values, both in terms of $\delta^{18}O$ and δD values (compilation by Hedenquist and Richards, 1998). Large ore deposits form as the result of a large fluid throughput, and in such a situation the water/rock ratios are too high to provide the necessary δD shift that would have to accompany a $\delta^{18}O$ shift of local meteoric water in order for this to be the dominant cause of the phyllic assemblage. Our results indicate a large magmatic hydrothermal cell about 2 to 3 km in diameter influenced the isotopic compositions of minerals through the late stage at El Salvador. This extended to the very late advanced argillic stage associated with formation of pebble dikes, although at this time there was significant involvement of meteoric water.

Advanced argillic assemblages: Exploration implications

Although pyrophyllite is by definition part of the advanced argillic assemblage (Meyer and Hemley, 1967), and locally does occur in equilibrium with an alunite-bearing assemblage in the very late stage breccias at El Salvador, it does not necessarily occur only in a sulfate-rich, alunite-forming environment. As noted by Hemley and Hunt (1992, pg. 40), assemblages characterized by hydrolytic alteration can form in two ways: (1) "[E]scape of the acid-rich, metal-poor vapor could produce extreme hydrolytic alteration on condensation"—i.e., the mechanism by which the very late advanced argillic quartz-alunite-(± accessory pyrophyllite-dickite-diaspore) assemblages formed (cf. Hedenquist et al., 1998). (2) In addition, in a retrograde situation, "lower temperature produces greater ionization of acidic constituents, and therefore . . . hydrolytic alteration will continue to occur and perhaps even intensify to produce advanced argillic assemblages." Thus, simple cooling of a solution during ascent can result in a transition from muscovite to pyrophyllite stability, and in a retrograde situation, preexisting muscovite may be replaced by pyrophyllite (Fig. 9) at quartz saturation.

Therefore, it is not surprising that the very late stage quartz-alunite assemblage, both as replacement and associated with pebble dikes, does not have an intimate association with the extensive zone of pyrophyllite overprint of muscovite at El Salvador (Figs. 4 and 5). A similar observation was made at the Far Southeast porphyry deposit (Hedenquist et al., 1998), where pyrophyllite forms on the margin of an illite halo to the porphyry deposit, underneath the higher elevation quartz-alunite replacement.

This distinction has significance for exploration. The quartz-alunite assemblage, called a lithocap by Sillitoe (1995), has a distribution controlled by a permeable lithology or fractures, and it overlies or caps the causative intrusive complex. Where these zones are preserved over a porphyry deposit there can be a large degree of lateral offset from the underlying parent stock (cf. Far Southeast-Lepanto; Hedenquist et al., 1998). This may be the case at El Salvador (Fig. 5), unless the quartz-alunite replacement is underlain by another causative intrusion. Thus, the location of an intrusion, and a potential porphyry deposit, may lie either beneath or subjacent to zones of quartz-alunite replacement. The distribution of these assemblages is controlled largely by the hydraulic gradient, which is affected by paleotopography (Sillitoe, 1995; Hedenquist et al., 1998).

By contrast, the pyrophyllite halo that forms from retrograde but nevertheless ascendant solutions, overprinting the phyllic assemblage, should reflect more closely the position of the underlying focus of the upflow (Sillitoe, 1995)—i.e., the latest intrusive stock responsible for circulation (Fig. 4). For this reason also, retrograde pyrophyllite commonly occurs much deeper than the quartz-alunite assemblage in situations that are unlikely to originate from so-called "acid drain back" of alunite-stable solutions (Hedenquist et al., 1998).

Conclusions

Surface mineral assemblages over the El Salvador porphyry deposit can be divided into a transitional to late stage, and a very late stage consistent with stages identified from underground studies. The transitional to late stage is characterized by assemblages of (1) muscovite-andalusite with trace diaspore, including some areas rich in andalusite, and (2) muscovite ± diaspore. There is a clear contact of muscovite-only outward to a marginal propylitic zone. Pyrophyllite occurs late in this stage as a retrograde overprint of muscovite. These assemblages are clearly zoned, centered on a core of least-altered L porphyry, a late intramineral intrusion of granodiorite. The muscovite-andalusite assemblage occurs up to 500 m away from the granodiorite porphyry, with andalusite-rich zones located near the brecciated margin of the porphyry. Further outward is the muscovite zone, from 500 to 1,500 m wide. The pyrophyllite overprint overlaps the contact of the muscovite-andalusite and muscovite zones, and it occurs largely above 3,000 m elevation such that its present distribution is controlled mainly by topography.

Very late stage assemblages are restricted to hydrothermal breccias and are dominated by a variable advanced argillic assemblage of alunite (± aluminum phosphate-sulfate or aluminum-phosphate minerals)-diaspore-zunyite-pyrophyllite-dickite. One of the breccia dikes extends upward into a 300 × 500 m outcrop of massive replacement quartz-alunite, forming an 80-m-thick cliff between Rhyolite Gulch and Granite Gulch. Other outcrops marked by limited replacement may occur elsewhere, but most alunite is related to the pebble dikes. Some supergene alunite and jarosite contain trace amounts of aluminum-phosphate minerals. This association is most likely caused by supergene sulfate replacement of hypogene alunite with aluminum-phosphate cores, the latter resistant to supergene dissolution. Indeed, the presence of such aluminum-phosphate minerals in supergene zones is strong evidence of a precursor hypogene alunite-bearing assemblage.

There is no clear isotopic zonation indicated by surface alteration at El Salvador that could have been applied to generate exploration guidelines here. The lack of any strong spatial zonation of isotopic compositions of the fluids responsible

for forming the muscovite or alunite may be due in part to the relative complexity of the hydrothermal system, caused by the multiple episodes of intrusion.

Large differences in the erosion level must be considered in any approach to exploration, whether geologic, geochemical, or geophysical. Clear isotopic zoning may be particularly evident where a strong hydraulic gradient existed at the paleowater table, resulting in a "spreading out" of the alteration, and where the quartz-alunite and silicic lithocap replacement is preserved in areas of relatively little erosion. Nevertheless, the degree of detail needed to properly assess isotopic results, plus the time and cost of analysis, will limit the usefulness and cost effectiveness of such study during the early stage of most exploration programs. For any such study to be reliable, there must be careful mapping of space-time relationships followed by collection and detailed preparation of mineral separates and a good understanding of paragenesis and paleotemperature; the latter information is seldom available during an exploration program.

By contrast, alteration zoning of porphyry systems has long been appreciated (Gilluly, 1946) and used successfully in exploration (Lowell and Guilbert, 1970), along with previously mentioned observations such as vein type, abundance and distribution, and the zoning of relict sulfides and supergene products. Mapping of relict alteration mineralogy (silicate, sulfate, and sulfide) in the field at El Salvador, backed up by laboratory checking of trace and residual mineralogy, is consistent with previous findings on subsurface zonation. For example, the andalusite-bearing areas at the surface correlate closely with hypogene copper ore that has a top at 200 to 300 m depth (Fig. 4), although this correlation may have resulted from the concentric intrusion of the late granodiorite porphyry after much of the ore was deposited. The common concentric emplacement of intrusions (Kirkham, 1971) means that there is typically a correlation between sericite and presericite ore zonation. However, this correlation may be largely fortuitous, such as at El Salvador. Thus, understanding the relationships between different intrusive stages and the potential for alteration zoning patterns to be uncoupled from ore distribution is essential for effective assessment of porphyry prospects.

These results gathered over the past 30 years from El Salvador can clearly be applied to porphyry exploration elsewhere. Careful mapping of hydrothermal assemblages, assisted by petrographic study, has the potential to identify subtle zoning. This zoning can help to locate the center of the intrusive system, even in situations where the surface mineralogy is largely phyllic in nature and has a strong supergene overprint. Nevertheless, the relationships derived from field mapping provide the fundamental guidelines for effective exploration and are an essential precursor to more detailed studies.

Acknowledgments

Permission to publish this study was granted by Francisco Camus, Corporación Nacional del Cobre de Chile (CODELCO), and by Yosuke Suzuki, Metal Mining Agency of Japan (MMAJ). The work was performed under a 1996 Memorandum of Agreement between CODELCO and MMAJ, with travel funding provided by MMAJ. We thank the geology department staff of El Salvador for their assistance and hospitality during fieldwork, Enrique Tidy of CODELCO for his support, and Hideya Metsugi and Kenichi Kurihara, MMAJ, for their assistance in the field. Stable isotope facilities at the Geological Survey of Japan (GSJ) were provided by Yukihiro Matsushisa, who was also the senior advisor to this project and who made the initial visit to the El Salvador mine to establish the outline of the project. We thank Rob King, GSJ, for assistance in the field, and for providing the kaolinite analyses, Eijun Ohta, GSJ Hokkaido Branch, for assistance with the microprobe studies, Akira Sasaki, GSJ, for help with S isotope analysis, and Hinako Shimizu, GSJ, for excellent technical assistance. We acknowledge the early workers at El Salvador who established the framework of understanding that contributed greatly to this project, and Julian Hemley, without whose experimental studies we would have been unable to fully interpret the mineralogical relationships. Dick Sillitoe initially suggested El Salvador as an ideal site for this study, helped to facilitate the initial agreement with CODELCO, and pointed out the location of the quartz-alunite zone to us. We thank Marco Einaudi for discussions on the topic, and Marco Einaudi, Lew Gustafson, Steve Matthews, Pepe Perelló, and Dick Sillitoe for their detailed reviews that improved the manuscript.

February 1, June 27, 2001

REFERENCES

Anderson, J.A., 1982, Characteristics of leached capping and techniques of appraisal, *in* Titley, S.R., ed., Advances in Geology of the Porphyry Copper Deposits, Southwestern North America: Tucson, University of Arizona Press, p. 275–295.

Arribas, A. Jr., 1995, Characteristics of high-sulfidation epithermal deposits, and their relation to magmatic fluid: Mineralogical Association of Canada Short Course Series, v. 23, p. 419–454.

Arribas, A., Jr., Cunningham, C.G., Rytuba, J.J., Rye, R.O., Kelly, W.C., Podwysocki, M.H., McKee, E.H., and Tosdal, R.M., 1995, Geology, geochronology, fluid inclusions, and isotope geochemistry of the Rodalquilar gold-alunite deposit, Spain: Economic Geology, v. 90, p. 795–822.

Clark, A.H., Archibald, D.A., Lee, A.W., Farrar, E., and Hodgson, C.J., 1998, Laser probe $^{40}Ar/^{39}Ar$ ages of early- and late-stage alteration assemblages, Rosario porphyry copper-molybdenum deposit, Collahuasi district, I region, Chile: Economic Geology, v. 93, p. 326–337.

Clode, C., Proffett, J., Mitchell, P., and Munajat, I., 1999, Relationships of intrusion, wall rock alteration and mineralisation in the Batu Hijau copper - gold porphyry deposit, *in* Weber, G., ed., PACRIM '99 Proceedings: Bali Indonesia, 10–13 October, 1999, Australasian Institute of Mining and Metallurgy Publication series no. 4/99, p. 485–498.

Cornejo, P., Tosdal, R.M., Mpodozis, C., Tomlinson, A.J., Rivera, O., and Fanning, C.M., 1997, El Salvador, Chile porphyry copper deposit revisited: Geological and geochronologic framework: International Geology Review, v. 39, p. 22–54.

Field, C.W., and Gustafson, L.B., 1976, Sulfur isotopes in the porphyry copper deposit at El Salvador, Chile: Economic Geology, v. 71, p. 1533–1548.

Frank, M.R., Candela, P.A., and Piccoli, P.M., 1998, K-feldspar-muscovite-andalusite-quartz-brine phase equilibria: An experimental study at 25 to 60 MPa and 400 to 550°C: Geochimica et Cosmochimica Acta, v. 62, p. 3717–3727.

Giggenbach, W.F., 1992a, Isotopic shifts in waters from geothermal and volcanic systems along convergent plate boundaries and their origin: Earth and Planetary Science Letters, v. 113, p. 495–510.

——1992b, Magma degassing and mineral deposition in hydrothermal systems along convergent plate boundaries: Economic Geology, v. 87, p. 1927–1944.

Gilluly, J., 1946, The Ajo mining district: U.S. Geological Survey Professional Paper 209, 112 p.

Gustafson, L.B., and Hunt, J.P., 1975, The porphyry copper deposit at El Salvador, Chile: Economic Geology, v. 70, p. 857–912.

Gustafson, L.B., and Quiroga G., J., 1995, Patterns of mineralization and alteration below the porphyry copper orebody at El Salvador, Chile: ECONOMIC GEOLOGY, v. 90, p. 2–16.

Gustafson, L.B., Orquera, W. McWilliams, M., Castro, M., Olivarez, O., Rojas, G., Maluenda, J., and Mendez, M., 2001, Multiple centers of mineralization in the Indio Muerto district, El Salvador, Chile: ECONOMIC GEOLOGY, v. 96, p. 325–350.

Hedenquist, J.W., and Richards, J.P., 1998, The influence of geochemical techniques on the development of genetic models for porphyry copper deposits: Reviews in Economic Geology, v. 10, p. 235–256.

Hedenquist, J.W., Matsuhisa, Y., Izawa, E., White, N.C., Giggenbach, W.F., and Aoki, M., 1994, Geology, geochemistry, and origin of high sulfidation Cu-Au mineralization in the Nansatsu district, Japan: ECONOMIC GEOLOGY, v. 89, p. 1–30.

Hedenquist, J.W., Arribas, A., Jr., and Reynolds, T.J., 1998, Evolution of an intrusion-centered hydrothermal system: Far Southeast-Lepanto porphyry and epithermal Cu-Au deposits, Philippines: ECONOMIC GEOLOGY, v. 93, p. 373–404.

Hemley, J.J., 1959, Some mineralogical equilibria in the system K_2O-Al_2O_3-SiO_2-H_2O: American Journal of Science, v. 257, p. 241–270.

Hemley, J.J., and Hunt, J.P., 1992, Hydrothermal ore-forming processes in the light of studies in rock-buffered systems: II. Some general geologic applications: ECONOMIC GEOLOGY, v. 87, p. 23–43.

Hemley, J.J., Montoya, J.W., Marinenko, J.W., and Luce, R.W., 1980, Equilibria in the system Al_2O_3-SiO_2-H_2O and some general implications for alteration-mineralization processes: ECONOMIC GEOLOGY, v. 75, p. 210–228.

Hunt, J.P., 1991, Porphyry copper deposits: ECONOMIC GEOLOGY MONOGRAPH 8, p. 192–206.

Kirkham, R.V., 1971, Intermineral intrusions and their bearing on the origin of porphyry copper and molybdenum deposits: ECONOMIC GEOLOGY, v. 66, p. 1244–1249.

Kusakabe, M., Hori, M., and Matsuhisa, Y., 1990, Primary mineralization-alteration of the El Teniente and Rió Blanco porphyry copper deposits, Chile. Stable isotopes, fluid inclusions and $Mg^{2+}/Fe^{2+}/Fe^{3+}$ ratios of hydrothermal biotite: University of Western Australia Publication 23, 16 p.

Losada-Calderón, A.J., and McPhail, D.C., 1996, Porphyry and high-sulfidation epithermal mineralization in the Nevados del Famatina mining district, Argentina, *in* Camus, F., Sillitoe, R.H., and Petersen, R., eds., Society of Economic Geology Special Publication 5, p. 91–117.

Lowell, J.D., and Guilbert, J.M., 1970, Lateral and vertical alteration-mineralization zoning in porphyry ore deposits: ECONOMIC GEOLOGY, v. 65, p. 373–408.

Metsugi, H., 1998, Extension of POSAM's on-site mineral identification to the green Cu minerals [abs.]: Pathways '98, Vancouver, Extended Abstract Volume, p. 233–236.

Meyer, C., and Hemley, J.J., 1967, Wall rock alteration, *in* Barnes, H.L., ed., Geochemistry of Hydrothermal Ore Deposits: New York, Holt, Rhinehart, and Winston, p. 166–232.

Mote, T.I., Becker, T.A., Renne, P., and Brimhall, G.H., 2001, Chronology of exotic mineralization at El Salvador, Chile, by $^{40}Ar/^{39}Ar$ dating of copper wad and supergene alunite. ECONOMIC GEOLOGY, v. 96, p. 351–366.

Ohmoto, H., and Goldhaber, M.B., 1997, Sulfur and carbon isotopes, *in* Barnes, H.L., ed., Geochemistry of Hydrothermal Ore Deposits—third edition: New York, John Wiley, p. 517–611.

Reyes, A.G., 1990, Petrology of Philippines geothermal systems and the application of alteration mineralogy to their assessment: Journal of Volcanology and Geothermal Research, v. 43, p. 279–309.

Reyes, A.G., Giggenbach, W.F., Saleras, J.R.M., Salonga, N.D., and Vergara, M.C., 1993, Petrology and geochemistry of Alto Peak, a vapor-cored hydrothermal system, Leyte province, Philippines: Geothermics, v. 22, p. 479–519.

Sheppard, S.M.F., and Gustafson, L.B., 1976, Oxygen and hydrogen isotopes in the porphyry copper deposit at El Salvador, Chile: ECONOMIC GEOLOGY, v. 71, p. 1549–1559.

Sheppard, S.M.F., Nielsen, R.L., and Taylor, H.P., Jr., 1969, Oxygen and hydrogen isotope ratios of clay minerals from porphyry copper deposits. ECONOMIC GEOLOGY, v. 64, p. 755–777.

Sheppard, S.M.F., Nielsen, R.L., and Taylor, H.P. Jr., 1971, Hydrogen and oxygen isotope ratios in minerals from porphyry copper deposits. ECONOMIC GEOLOGY, v. 66, p. 515–542.

Sillitoe, R.H., 1973, The tops and bottoms of porphyry copper deposits: ECONOMIC GEOLOGY, v. 68, p. 799–815.

——1995, Exploration of porphyry copper lithocaps: Pacrim Congress 1995, Auckland New Zealand, Australasian Institute of Mining and Metallurgy, p. 527–532.

Stoffregen, R.E., and Alpers, C.N., 1987, Woodhouseite and svanbergite in hydrothermal ore deposits: Products of apatite destruction during advanced argillic alteration: Canadian Mineralogist, v. 25, p. 201–211.

Sverjensky, D.A., Hemley, J.J., and D'Angelo, W.M., 1991, Thermodynamic assessment of hydrothermal alkali feldspar-mica-aluminosilicate equilibria: Geochimica et Cosmochimica Acta, v. 55, p. 989–1004.

Taylor, B.E., 1992, Degassing of H_2O from rhyolite magma during eruption and shallow intrusion, and the isotopic composition of magmatic water in hydrothermal systems, *in* Hedenquist, J.W., ed., Magmatic Contributions to Hydrothermal Systems: Geological Survey of Japan Report 279, p. 190–194.

Taylor, H.P. Jr., 1974, The application of oxygen and hydrogen isotope studies to problems of hydrothermal alteration and ore deposition. ECONOMIC GEOLOGY, v. 69. p. 843–883.

——1997, Oxygen and hydrogen isotope relationships in hydrothermal mineral deposits, *in* Barnes, H. L., ed., Geochemistry of Hydrothermal Ore Deposits—third edition: New York, John Wiley, p. 229–302.

Wasserman, M.D., Rye, R.O., Bethke, P.M., and Arribas, A., Jr., 1992, Methods for separation and total stable isotope analysis of alunite: U.S. Geological Survey Open-File Report 92-9, 20 p.

Watanabe, Y., and Hedenquist, J.W., 1998, Mineralogical and stable isotope zoning of surface alteration at the El Salvador porphyry Cu deposit: Application to exploration: Geological Survey of Japan Open-File Report 376, 62 p.

Watanabe, Y., Stein, H.J., Morgan, J.W., and Markey, R.J., 1999, Re-Os geochronology brackets the timing and duration of mineralization for the El Salvador porphyry Co-Mo deposit, Chile [abs.]: Geological Society of America Annual Meeting, Abstracts with Program, v. 30, p. A30.

APPENDIX

Sample and Analytical Methods

In order to determine the mineralogical assemblage, paragenesis, and zoning, we mapped and collected 276 samples from 203 surface localities in an area of >5 km^2 at an elevation of 2,900 to 3,300 m (JES series; Fig. A1). In addition, we collected a suite of samples from the El Salvador sample library at the mine (ES series) from areas currently inaccessible (sample descriptions in Watanabe and Hedenquist, 1998). Five samples of supergene kaolinite in drill core were collected from shallow drill holes.

These samples were first analyzed in the field by hand lens and scratcher, and later in the mine office by a portable spectrometer (POSAM; Metsugi, 1998). Later they were cut, the rock types described, and the major alteration minerals were checked with X-ray diffraction (XRD). In most cases the samples for XRD analysis were removed from the rock samples with a dental drill. Phenocryst alteration was preferred for separation and XRD analysis, but if a sample did not contain large enough phenocrysts, groundmass material or a bulk rock sample was used, although in these cases supergene minerals commonly were dominant. Some clay minerals were purified by hydraulic elutriation after hand picking (Wasserman et al., 1992), to aim for >95 percent purity before isotopic analysis of silicates. The mineral assemblage and paragenesis of selected samples were examined by microscope in thin sections and polished thin sections. Some polished sections were also used for qualitative chemical analysis by electron probe microanalysis, and for back-scattered electron imaging.

Muscovite, pyrophyllite, kaolinite and alunite samples were prepared for O and H isotope analysis (plus S isotopes on alunite, jarosite, barite and pyrite) by handpicking, using needles for samples with alteration of large phenocrysts (>3 mm). If the sample did not contain large phenocrysts, it was crushed and clay minerals were separated by hydraulic elutriation. Muscovite separates were >4μm in size, whereas dickite and kaolinite fractions were <2μm. Most samples were essentially pure (>95%). However, in some samples both muscovite and

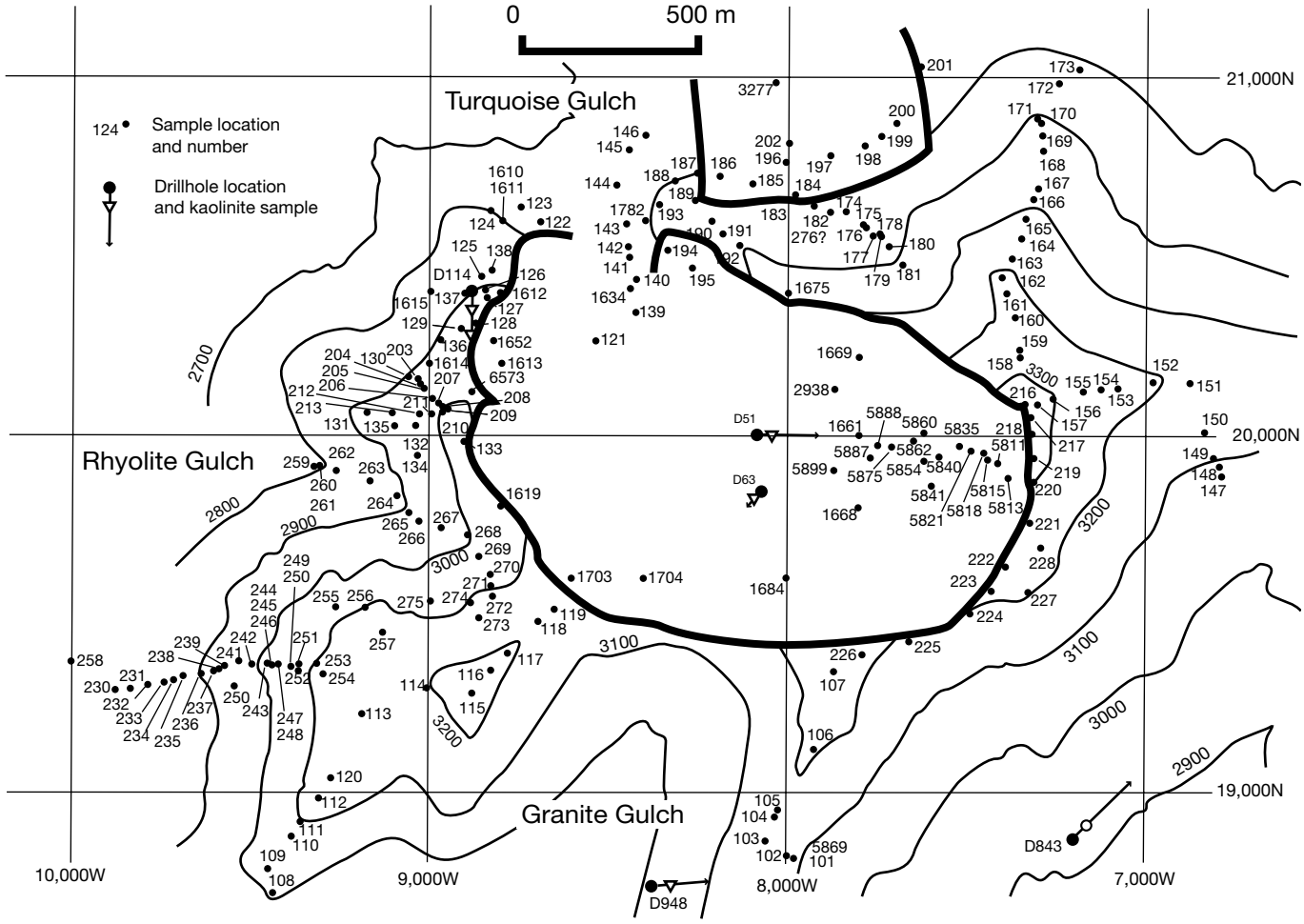

FIG. A1. Location map of surface samples and the surface drill holes (Dxxx) from which supergene kaolinite samples were collected. Samples with a three-digit number are from our collection, whereas samples with a four-digit numbers are from the El Salvador library. Grids are 1,000 m square.

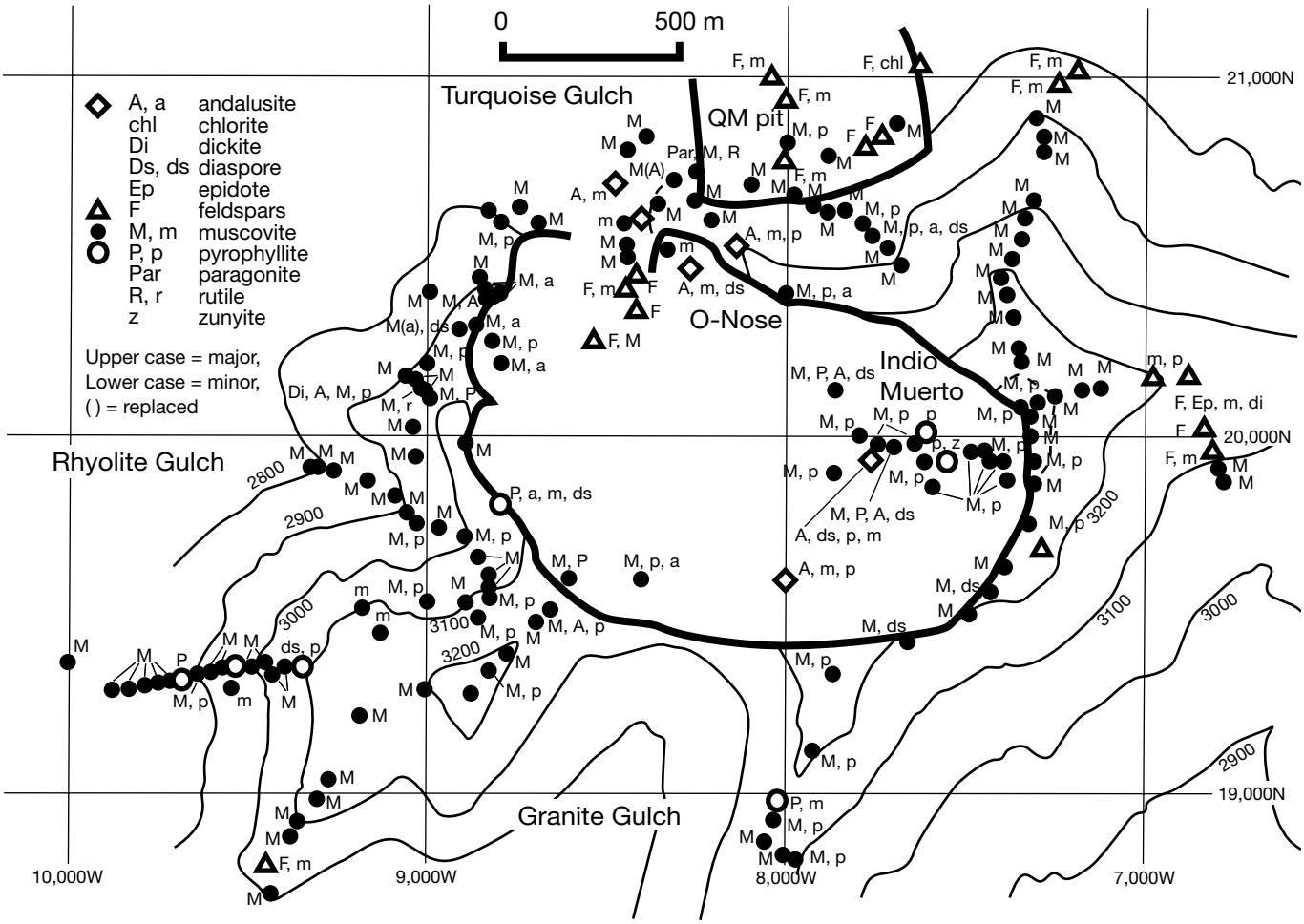

FIG. A2. Transitional to late stage assemblages of wall-rock samples from the surface. These data were used to estimate the temperature in order to calculate isotopic fractionation factors (Tables 1 and A1).

pyrophyllite were present, and in these cases, the proportion of pyrophyllite was estimated by XRD (Watanabe and Hedenquist, 1998). Hypogene samples for which XRD showed more than a trace (>5%) of kaolinite were generally discarded.

Alunite samples were prepared for O (and some for S) isotope analysis by first dissolving the alunite in 0.5 N NaOH at 80°C; sulfide does not dissolve under these conditions and remains as a residue. The sulfate was precipitated as barite after acidifying to pH 2.8 (Wasserman et al., 1992). The original alunite, precipitated barite, and residual pyrite were prepared for S isotope analysis by the KIBA dissolution method. A good agreement between the alunite and precipitated barite analyses indicates that the initial alunite samples did not contain more than a trace of sulfide. The residue after dissolution was examined by XRD, and some samples from breccias were found to contain aluminum-phosphate minerals (crandallite and florencite; Table A1), insoluble in the NaOH, that existed as cores of the laboratory-dissolved sulfate minerals.

In total we analyzed the isotopic composition of 48 surface samples of silicate minerals: muscovite (37), pyrophyllite (2), dickite (2), and supergene kaolinite (7). All were analyzed for their $\delta^{18}O$ value, but only 24 muscovite samples were analyzed for δD composition. Twenty sulfate minerals were analyzed: alunite (18), jarosite (1), and barite (1). Four of the alunite samples are supergene in origin, as indicated by their light S isotope composition, similar to sulfide; pyrites from two of these samples were also analyzed. In addition to S isotopes, 13 of the alunites, one supergene in origin, and the supergene jarosite were also analyzed for both $\delta^{18}O$ and δD composition. Isotopic analyses were made at the Geological Survey of Japan following the procedures outlined by Hedenquist et al. (1998). Thirteen samples had one or more isotopic analysis duplicated. On the basis of replicate analysis of standard minerals, the reproducibility was typically ±0.1 per mil $\delta^{18}O$, ±2 per mil δD, and ±0.2 per mil $\delta^{34}S$.

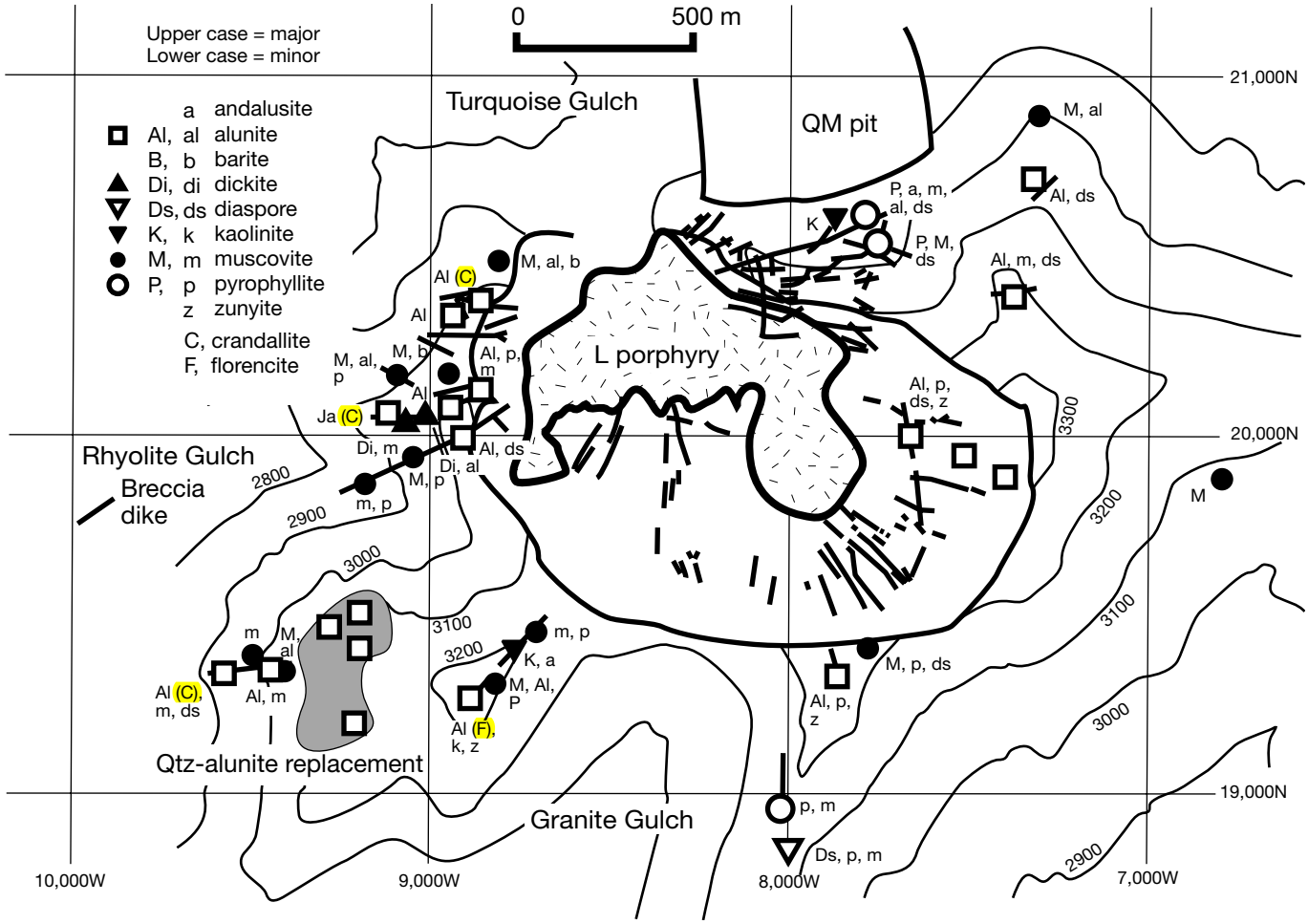

FIG. A3. Very late stage assemblages associated with hydrothermal breccia and quartz-alunite replacement samples from the surface. These data were used to estimate the temperature in order to calculate isotopic fractionation factors (Tables 1 and A1).

TABLE A1. Mineral Assemblages and Isotopic Compositions of Mineral Separates[1]

Sample number	Mineral analyzed	Assemblage	$\delta^{18}O$ (‰)	δH (‰)	H_2O (wt%)	$\delta^{34}S$ (‰)	T (°C)	$\delta^{18}O$ H_2O	δH H_2O
105a	Alunite					(14.9, 14.8)			
107c	Alunite	Al-APS	9.1, 8.6	–49		12.2 (13.2)	250	0.5	–43
111	Muscovite	M ± Dsp	8.2	–58	4.6		325	5.3	–33
112	Muscovite		8.3						
113	Alunite	Lithocap				14.8			
115c	Alunite	Al-APS, F residue	11.4	–40		18.3	250	3.0	–34
116	Muscovite + P		8.0						
119b	Muscovite	M-Dsp-P	9.2	–79	4.5		300	5.7	–53
127	Muscovite	A-M-Dsp	8.4	–61	4.0		375	6.5	–36
129	Muscovite	A-M-Dsp	9.5	–59	4.4		375	7.6	–34
130b	Muscovite	M ± Dsp	8.4	–66	4.4		325	5.5	–41
130b	Alunite, S					1.4			
133a	Muscovite		8.2						
134	Muscovite		8.0						
135	Dickite		7.8	–70	13.5		150	–0.9	–50
138	Alunite Sg	C in residue	(8.5)	–46		–1.9, –2.1			
147	Muscovite		7.4						
155	Muscovite	M ± Dsp	7.8, 8.0	–62, –63	4.7, 4,7		325	5.0	–38
160	Muscovite		8.3						
163a	Muscovite		7.5						
166	Muscovite	A-M-Dsp	9.9, 10.0	–65	5.0		325	7.0	–40
170	Muscovite	M	11.6	–62	4.4		250	6.6	–37
177	Muscovite	A-M-Dsp	8.0	–63	4.1		375	6.1	–38
189	Muscovite	A-M-Dsp	10.3	–60	4.2		375	8.4	–35
194	Kaolinite, Sg		13.8	–86	11.9		25	–10.5	–53.5
							35	–8.5	–55
197	Alunite Sg					0.0			
	Pyrite					–3.2			
200	Muscovite	M	11.1	–61, –64	4.1, 4.4		250	6.1	–38
205	Muscovite	M ± Dsp	8.4, 8.4	–53, –57	4.8		325	5.5	–30
207	Muscovite:P, 2:1		8.9						
208	Barite					12.1			
209	Muscovite:P, 2:1		8.2						
211	Alunite, early	Al	9.6	–47		18.4	200	–1.3	–41
	Alunite, late		10.6	–42		18.8 (18.5)		–0.3	–36
212	Dickite		11.5	–78	13.5		100	–1.6	–54
213b	Jarosite	C in residue	5.4	–96		–2.1			
218	Muscovite	M ± Dsp	8.0	–65	4.0		325	5.1	–40
219	Muscovite	M ± Dsp	8.0	–71, –72	4.0, 4.1		325	5.1	–47
220	Muscovite		6.8						
221	Muscovite		8.3						
222	Muscovite	M ± Dsp	8.2	–63	4.3		325	5.3	–38
225	Muscovite	M ± Dsp	8.4	–68	3.4		325	5.5	–43
226	Muscovite	M-Dsp-P	8.7	–71	4.1		300	5.2	–46
227	Muscovite	M ± Dsp	8.5	–68	3.9		325	5.6	–43
238	Alunite	Al-APS-Dsp	11.9	–43		9.6 (9.9, 10.3)	300	5.4	–33
243a	Muscovite	M ± Dsp	8.3, 8.6	–62	4.4		325	5.6	–37
244	Alunite	Al	11.8	–38		(15.5)	200	0.9	–32
255	Alunite	Al, lithocap	12.1	–42		16.3 (16.7)	200	1.2	–36
256	Alunite	Al, lithocap	12.0	–46		(16.1)	200	1.1	–40
257	Alunite	Al, lithocap	11.4	–43		(14.4)	200	0.5	–37
263a	Muscovite	M ± Dsp	8.1	–60	4.5		325	5.2	–35
270	Muscovite	M ± Dsp	7.6	–68	5.1		325	4.7	–43
271	Muscovite	M ± Dsp	8.0	–75	4.4		325	5.1	–50
1669	Muscovite	A-M-Dsp	7.9	–70	3.8		375	6.0	–45
1675	Muscovite	A-M-Dsp	8.5	–64	3.3		375	6.6	–39
1703	Muscovite		7.9						

TABLE A1. *(Cont.)*

Sample number	Mineral analyzed	Assemblage	$\delta^{18}O$ (‰)	δH (‰)	H_2O (wt%)	$\delta^{34}S$ (‰)	T (°C)	$\delta^{18}O$ H_2O	δH H_2O
3183	Alunite Sg					–4.7			
	Pyrite					–5.2			
5815	Alunite	Al-M-P-goethite				(15.5)			
5821	Pyrophyllite	P	6.7	–71	5.1		300	3.2	–46
5835	Alunite	Al-APS-Dsp	8.0	–55		(17.7)	300	1.5	–45
5860	Alunite	Al-APS-Dsp	7.6	–45		(15.7, 15.2)	300	1.1	–35
5875	Pyrophyllite + A	P after A	11.8						
5888	Muscovite		6.5						
6573	Alunite	Al-APS-Dsp-P	6.4	–42		(14.8)	300	–0.1	–32
6573	Pyrophyllite[2]	Al-P	8.7	–51	5.0		300	5.2	–26
D51-01	Kaolinite, S		15.1	–99			25	–9.2	–66.5
							35	–7.2	–68
D76-10	Kaolinite, Sg		15.1	–87			25	–9.2	–54.5
							35	–7.2	–56
D114-01	Kaolinite, Sg		10.4				25		
							35		
D114-09	Kaolinite, Sg		12.7	–89			25	–11.6	–56.5
							35	–9.6	–58
D843-09	Kaolinite, Sg		15.8	–83			25	–8.5	–53.5
							35	–6.5	–52
D948-03	Kaolinite, Sg		12.4	–96			25	–11.9	–66.5
							35	–9.9	–65

All muscovite and pyrophyllite from the transitional to very late stage, and all alunite and dickite from the very late stage; the temperature estimate used for calculating the isotopic composition of the fluid is based on the mineral assemblage (Table 1); fractionation factors from Hedenquist et al. (1998), their appendix 1

Abbreviations: A = Andalusite, Al = Alunite, APS = Aluminum-phosphate-sulfate mineral, C = Crandallite (aluminum-phosphate mineral), D = drill hole sample, Dsp = Diaspore, F = Florencite (aluminum-phosphate mineral), J = jarosite, M = Muscovite, P = Pyrophyllite, Sg = supergene, ( ) = S isotope value obtained from sulfate mineral digested by KIBA, not processed by NaOH

[1] Table A1: Isotopic results of muscovite and other silicate minerals from surface samples; mineral assemblages (Figs. A2 and A3) used to estimate temperatures (Table 1) for isotopic calculations are listed; the V-SMOW values were established relative to internal standards, which included NBS-28 quartz, 9.34 per mil $\delta^{18}O$, and Misasa muscovite, –60 per mil δD; reproducibility, on the basis of replicate analysis of standards, was typically ±0.1 per mil $\delta^{18}O$ and ±2 per mil δD

Isotopic results of alunite and related S-bearing minerals from surface samples are also tabulated; the S isotope results for alunite were obtained from samples dissolved in hot NaOH and reprecipitated as barite, thus eliminating any contamination by sulfide; results for alunite samples prepared directly by KIBA digestion are listed in parentheses; there is typically very good correlation between the two preparation methods, indicating very little if any sulfide contamination in the alunite samples; the V-CDT and V-SMOW values quoted have been established in comparison with internal standards, which include, respectively, SS standard Ag_2S, –2.36 per mil $\delta^{34}S$ (for all S-bearing minerals), and San Gregorio barite, 9.1 per mil $\delta^{18}O$ (for all sulfates); reproducibility was typically ±0.1 per mil $\delta^{18}O$ and ±0.2 per mil $\delta^{34}S$

[2]Pyrophyllite with alunite in breccia dike, sample 6573, analyzed by Sheppard and Gustafson (1976)